AP-E001180

LEVEL II

SECURITY CLASSIFICATION OF THIS PAGE (When Data Entered)

REPORT DOCUMENTATION PAGE

READ INSTRUCTIONS BEFORE COMPLETING FORM

1. REPORT NUMBER	2. GOVT ACCESSION NO.	3. RECIPIENT'S CATALOG NUMBER
Annual Technical Report	AD-A106753	

4. TITLE (and Subtitle)	5. TYPE OF REPORT & PERIOD COVERED
Stability of Optical Coatings in Hostile Excimer Laser Environments	Annual Technical Report 7/1/80 - 6/30/81
	6. PERFORMING ORG. REPORT NUMBER
7. AUTHOR(s)	8. CONTRACT OR GRANT NUMBER(s)
Ansgar W. Schmid	N00014-80-C-0798
9. PERFORMING ORGANIZATION NAME AND ADDRESS	10. PROGRAM ELEMENT, PROJECT, TASK AREA & WORK UNIT NUMBERS
Department of Physics Washington State University Pullman, WA 99164	
11. CONTROLLING OFFICE NAME AND ADDRESS	12. REPORT DATE
Office of Naval Research Physics Program 800 N. Quincy Street, Arlington, VA 22217	August 31, 1981
	13. NUMBER OF PAGES 39
14. MONITORING AGENCY NAME & ADDRESS (if different from Controlling Office)	15. SECURITY CLASS. (of this report) Unclassified
	15a. DECLASSIFICATION/DOWNGRADING SCHEDULE

16. DISTRIBUTION STATEMENT (of this Report)

Approved for public release; distribution unlimited

DTIC ELECTE NOV 0 5 1981 S

17. DISTRIBUTION STATEMENT (of the abstract entered in Block 20, if different from Report)

18. SUPPLEMENTARY NOTES

19. KEY WORDS (Continue on reverse side if necessary and identify by block number)

optical thin films, dielectric coatings, UV laser mirror, excimer laser, silicon dioxide, laser damage, chemical sputtering, laser materials

20. ABSTRACT (Continue on reverse side if necessary and identify by block number)

E-beam evaporated SiO_2 films were investigated during and after exposure to XeF laser gas components. Experimental methods and results are described, indicating that i) impurities in the films reduce chemical film stability even without laser photons present; ii) low energy ions from the laser plasma enhance film decomposition; iii) mirror substrate temperature between room temperature and 100°C does not influence etching significantly.

DD FORM 1 JAN 73 1473 EDITION OF 1 NOV 65 IS OBSOLETE
S/N 0102 LF 014 6601

SECURITY CLASSIFICATION OF THIS PAGE (When Data Entered)

8111 03 038

AD A106756

DTIC FILE COPY

PREFACE

Excimer lasers operating with halogen based gain media pose peculiar material problems. Not only do their UV lasing wavelengths reach into the absorption edge tails of many optical materials, but their applications frequently demand design features which bring the optical components into direct contact with the excited gain medium and thereby subject the optical component surfaces to chemical attack by laser-fuel constituents. It is the purpose of this study to shed light onto this chemical attack which usually happens while lasing occurs, i.e., while intense x-ray and UV photon fluxes are present. Experience shows that these effects greatly limit the optical components' useful life before failure and thus render the total excimer laser system less than desirable.

This report covers all activities aimed at an understanding of synergistic effects during the first year of contract N00014-80-C-798.

Synergistic effects are defined here as combined effects by two or more reaction participants such as excimer gas constituents together with UV photons, x-rays, low energy electrons, or ions. It is the ultimate goal of this effort to elucidate the relative effectiveness of such synergistic optical component decomposition mechanisms on different UV mirror coatings. The first engineering oriented phase of the program will be described here.

The following individuals contributed to the effort during 1980-81:

Dr. Ansgar Schmid, Principal Investigator

Dr. J. Thomas Dickinson, Principal Investigator

Michael Loudiana, Graduate Research Assistant

Rob Townsley, Undergraduate Assistant

Kyle Bell, Undergraduate Assistant

BACKGROUND

UV laser mirrors are presently being investigated for several reasons. Aside from the chemical problems to be described here, large scale XeF lasers introduce demands on mirrors which are particularly stringent in terms of thermal distortion, surface finishing and light scattering properties among other features. The most prominent characteristics of chemical interest are the dielectric nature of mirror coatings and their respective microtopography. Currently a variety of compounds are under investigation which will result in the emergence of an optimal mirror coating material which can live up to all chemical, as well as other, before mentioned, demands. Among the most promising such materials one presently finds SiO_2, MgF_2, and cryolite.

All chemical survival studies under this contract up-to-date have focused on SiO_2. This choice was mandated by the simple fact that SiO_2 performs well in many other regards and has therefore become the prime candidate for half-wave block (the top half-wave layer on many multi-stack dielectric UV coatings). Being the uppermost layer the half-wave block will be the first surface to face chemical radicals impinging from the laser excitation region. However, improved deposition procedures seem to develop other materials into viable competitors for SiO_2's role in the half-wave block. Such materials will be investigated as soon as studies on SiO_2 are reasonably complete and methodologically of sufficient confidence level.

Prior to the start-up of SiO_2 experiments the relevant components of XeF excitation gas mixtures were identified. These are based on XeF laser operation at 3 amagat with Xe and NF_3 as primary fuels and a light rare gas as buffer. A brief report[1] on KrF discharge components finds, at least for small scale units, chemical lasing by-products of the type NF_2, NF, and F. Additional components such as XeF_2 can be formed under favorable conditions,

such as at elevated temperatures and pressures,[2] conditions typically found in advanced, large scale XeF systems. It was therefore the first program task to develop equipment systems for generating these discharge components individually. Monitoring of chemical activity by these individual components on SiO_2 surfaces is achieved by several quantitative and qualitative methods: during exposure of SiO_2 films by a quartz microbalance technique in conjunction with visible optical microscopy, and after exposure by independent scanning electric microscopy. One can envision a wide variety of situations where interaction of lasing gases with solid dielectric surfaces would require more sophisticated surface analytical techniques. A significant effort was therefore directed towards establishing a SIMS (secondary ion mass spectrometry) facility which will, during the second phase of the program, be employed together with already existing surface analytical tools, i.e., Auger spectroscopy, quadruple mass spectrometry, etc. With the equipment in place, NWC supplied 1000 Å SiO_2 coatings were analyzed in the presence of a molecular beam of XeF_2 and of an atomic beam of F. The details of these measurements will be described later. First we will describe the experimental facilities which were built and tested during the 1980-1981 contract period, then the experimental data will be presented and, in the end, future work will be outlined.

EXPERIMENTAL FACILITIES

The first year program instrumentation objective was two-fold: build F and NF_x sources for exposure of SiO_2 and use commercially available XeF_2 on SiO_2 for quick data gathering during that build-up phase. All data were taken by quartz crystal microbalance mass loss measurements.

The 1000 Å SiO_2 films were evaporated by NWC onto vendor supplied silver coated resonator crystals. From an initial batch of 100 crystals, specimens were selected according to certain frequency shift-temperature characteristics and supplied to NWC for film deposition. This selection process proved useful in eliminating frequency shifts during exposure to XeF_2 from being attributed to exothermic effects rather than to mass variation. By keeping the resonator crystal temperature constant by water cooling, the SLOAN crystal mount mass removal sensitivities of the order of less than a monolayer can confidently be maintained. This sensitivity requirement was routinely tested by low energy Ar^+ sputtering of both Si and SiO_2 films for which such sputtering yields are documented. The SLOAN crystal mount was positioned inside a stainless-steel UHV system so that the test sample could simultaneously be exposed to an electron beam, an Ar^+ ion beam and the molecular XeF_2 beam. This setup permits further irradiation of the sample with UV light under grazing incidence through an 8" sapphire window. In addition to the mass loss measurement an UHV system port positioned 120° relative to the molecular beam direction allows for attachment of a UTI or FINNIGAN quadrupole mass spectrometer and thus for constant residual gas analysis and measurement of surface etch products entering the gas phase. On the basis of tests with pure Si films we are justified in believing that the two independent measurements, mass loss and quadrupole mass spectroscopy, agree to within 50%. For a detailed explanation of this rather unsatisfactory agreement see the section "Results and Data Analysis."

Analysis of SiO_2 film impurity contents was performed by a cylindrical mirror Auger analyzer (VARIAN), which was positioned such that the sample had to be removed from the quartz crystal mount and transferred to a separate carousel manipulator. Auger analysis was therefore done either ahead of or after exposure to XeF_2.

XeF_2 supplied by PCR is a small grained, white powder with a vapor pressure of about 3 Torr at room temperature. The substance was transferred from its shipping vessel to a stainless-steel reservoir within an Ar atmosphere glove box. As a consequence, large amounts of Ar as well as of Xe had to be pumped during exposure measurements with the undesirable result that often, even for D.I. ion pumps, the pumping efficiency became degraded to the point where uncontrolled pressure fluctuations ("burping") rendered measurements meaningless. The rare gases are now, however, effortlessly pumped by the cryogenic back-up pump which for that purpose had especially been designed in-house by scavanging a 5W closed-cycle refrigeration cryostat from a spectroscopy setup and mating it with a commercially obtained 3π Chevron array (VARIAN). The tandem operation of the 400 ℓ/sec D.I. ion pump with the 5W cryopump produced a pressure differential of about 180:1 between the end of the 1/32" stainless-steel tube which introduced the XeF_2 into the system and the background pressure. The background pressure was always maintained low enough for the quadrupole mass spectrometer to be able to detect the minute partial pressures of reaction products, such as SiF_3.

During the course of the experiment it was found that "as supplied" XeF_2 contains unidentified impurities which initially inhibit etching of both Si and SiO_2 films by building up a surface layer. This build-up manifests itself by a characteristic, steady decline in resonance frequency of the microbalance as well as by a conspicuous absence of detectable traces of etch

products in mass spectroscopy. The rate of buildup was found to be different for dielectric films as opposed to pure Si films and is presently not well understood. Further investigation of this phenomenon will resume with the coming on-line of the SIMS apparatus. One earlier explanation for this phenomenon, viz., the chemisorption of reaction products stemming from the gas feed system's wall interacting with the XeF_2, could be discarded after thorough passivation of all walls by F_2 gas did not affect the apparent deposition.

A practical remedy against the obscure film deposition was found in long term cryodistillation of XeF_2. By pumping on the XeF_2 reservoir while it was cycled through sequences of constant temperature baths (methyl cyclopenthane slush - 142.4°C, ethanol slush - 117.3°C, chloroform slush - 64°C, CCl_4 slush - 24°C) for many hours, build-up periods for the unknown films could be dramatically reduced. Note that the XeF_2 leak-in system was not differentially pumped after all forepump oils, including fluorinated compounds like Fomblin, showed a significant tendency to polymerize on copper and stainless-steel surfaces when brought into extended contact with XeF_2. As standard practice, the cooled reservoir was attached to a Granville-Phillips precision leak-valve which on the high pressure side was also connected to a thermocouple gauge. The XeF_2 molecular flow through the valve was controlled by setting the leak-valve once and thereafter by changing the temperature of the reservoir. Cryo-distillation of XeF_2 before use and direct attachment of the reservoir to the chamber led to satisfactory etching behavior. Therefore, there is little reason to believe that the before-mentioned film deposition was due to quantities of gaseous impurities which were produced during wall reactions of XeF_2 with the stainless-steel chamber.

In order to study the effects which low energy ions or low energy electrons may cause in conjunction with XeF_2 and other lasing components,

care had to be taken [illegible] introduce additional intangibles by using clean designs for the respective devices. It is, for instance, widely accepted that hot-filament electron guns severely contaminate nearby samples. We therefore decided to develop an electron source which uses a channeltron electron multiplier array (spiraltron array) in reverse. By operating the device in the upper range of its recommended operating voltage interval the inherent noise of the device results in current densities of 3×10^{-7} A/cm^2 without any further input into the device. The ion gun is a commercial model obtained from VARIAN.

A. Atomic F Source

While useful information was gained from the interaction studies of SiO_2 with XeF_2, an apparatus for production of F atoms was developed. It is based on the dissociation of F_2 molecules in an RF discharge which is a very popular and highly efficient method.[3] Most other homonuclear diatomic molecules are known not to completely dissociate in RF discharges. F_2 constitutes a notable exception because of its large dissociative attachment cross section for thermal electrons.[4] Dissociation is further enhanced by the F atoms slow rate of homogeneous recombination. However, in spite of reports in the literature claiming 100% dissociation in microwave discharges, production of F atoms by RF or microwave discharges is not without drawbacks when applied to surface reaction studies on substances such as SiO_2.

Due to the extremely reactive nature of atomic fluorine, great caution is mandated in the choice of materials which will contact the atoms. Two severe problem areas were identified during the course of these studies and solutions were found.

The first problem area was contamination from electrode materials. This problem lends itself to a simple solution by applying the RF power to electrodes located outside the reaction vessel.

The second problem area is more intrinsic in that atomic F very readily attacks Pyrex, a desirable material for the discharge vessel wall since it permits easy visual observation and control of the discharge. Not only does that reaction lead to copious amounts of SiF_4, the same substance being used as marker for reactions taking place on the optical coating specimens, it also renders the vessel walls opaque after only brief periods of operation. Strong air cooling of the vessel walls to reduce the temperature and thereby the reaction role was not found successful in sufficiently reducing contamination. However, by sacrificing visibility of the discharge, alumina tubes can be used which we believe to form nonvolatile aluminum fluoride.[5] Whether a higher power (above 100W) RF discharge will render this species unstable we cannot decide, but aside from some atomic oxygen no other reaction products were found mass spectroscopically when the alumina tube discharge vessel was operated at 100W. No air cooling was provided in that instance. Unfortunately, the attractive features of high purity Al_2O_3 (Coors 995) are lost in the difficulty of forming a temperature compatible, chemically stable ceramic to metal transition. This very intricate joining work was done by Dr. Ben Rosenblum[7] of the Kansas City Division of the Bendix Corporation at no cost to the contract. The materials and methods used in that effort are considered proprietary. The manufactured joint links the 1" O.D. alumina vessel to the all stainless-steel vacuum chamber. Fluorine atoms, and possibly ions, emanate from the discharge region through a 0.006" alumina orifice into an E-field region provided to remove any charged components emanating from the source.

The composition of the atomic beam was analyzed by an EXTRANUCLEAR Model #061-1 quadrupole mass analyzer. After moderately long periods of operation, this and a substitute mass spectrometer inhibited data taking in a

continuous fashion. The high background problem is presently being solved by pulsing the RF discharge and by employing phase-sensitive detection.

Since the RF oscillator is usually run at plate voltages between 600 and 1000 V, a high voltage switch with power-handling capabilities of 100W had to be designed. The circuit for that purpose shown in Fig. 1 combines both simplicity and speed with logic element interfacibility. The key elements of the circuit are three cascaded high voltage power transistors (DTS 801) which are simultaneously switched by respective optically isolated trigger circuits. Sections (b) and (c) of Fig. 1 show one isolated trigger stage.

Currently there are several types of transistors offered which all can withstand a collector-emitter voltage of 1000 V at reasonable switching speeds. Note, however, that the advantage in circuit simplicity, i.e., a single switch instead of three stages, is in all cases traded off against a power limit which in turn limits the safe collector current to values that are insufficient to drive the RF plasma. We consider our design a proper balance between these requirements.

An external trigger source activates the parallel switched optocouplers. Jitter and differences in risetimes among the three optocouplers are trimmed by 250Ω potentiometers. The string of driver stages is statically protected by a voltage-sharing network of 35 kΩ resistors which insure that no single stage is overvoltaged because of unequal leakage currents.

With careful trimming and driven by TTL pulses the circuit delivers pulses with risetimes of less than 5 μsec into noninductive loads. Since the oscillator, a commercial unit ORTEC Model 307, operates at a fixed frequency of 13.6 mHz switching of the plate voltage at a rate of less than 400 Hz

is entirely sufficient for full power to be delivered to the discharge and for a standard lock-in amplifier to lock on to.

The experimental chamber housing the quadrupole analyzer is kept in the low 10^{-6} Torr range by a 600 ℓ/sec BALZERS oil diffusion pump while the ion source vessel is at a few full operating pressure (~ 0.5 Torr). In this mode no differential pumping was required on the discharge vessel itself and pressure regulation by simple stainless-steel needle valve controls on the gas inlet post was found entirely sufficient.

Unanticipated delays in bringing the F source to full operation during the first year are mainly due to the difficulty in switching from a Pyrex discharge vessel to an alumina one and to the corresponding problem of developing a high temperature, vacuum tight, chemically compatible alumina to stainless-steel seal. This thorny problem was ultimately solved by falling back on extramural expertise.

B. SIMS Facility

The quadrupole based secondary ions mass spectrometer is presently in its final stages of assembly. Its design was governed by the interest of having a facility which is both portable in terms of its primary beam source, and dedicated to be used only in conjunction with reacting optical thin film samples in terms of the secondary ion quadrupole analyzer. That is to say, the primary ion source is to be easily decoupled and used on other experiments, if such need arises, and the overall design did not have to take account of spatial requirements by any other surface analytical instruments, i.e., Auger analyzer, LEED system, which frequently are used as a combination of techniques in surface studies. Such a modular design brings about another advantage: with the sample placed in a different chamber than the primary

ion source differential pumping of the two separate chambers will permit analyzing the sample under UHV conditions.

The primary ion gun column is a commercial coloutron ion gun (Coloutron Corp., Boulder, CO) pumped by a 1400 ℓ/sec BALZERS horizontal turbomolecular pump and cooled by a closed Freon-11 cycle.

This pump and its mechanical forepump are mounted together as an independent station with only a bellows coupling connecting the sample chamber with the gun body. A special control unit was developed in-house which operates both pumps and associated valves in such a manner that power outages will trigger a prescribed shut-down of the system without harmful contamination of the chambers by backstreaming forepump oil. Such precautions have on several occasions proved to be of fundamental importance. An outline of the control circuits is shown in Figs. 3

Two months after receipt of the ALCATEL forepump a mechanical dysfunction in the vane section of the pump required lengthy warranty procedures which appreciably slowed progress of the SIMS development. Presently a low pumping speed mechanical pump substitutes in a make-shift arrangement.

The secondary ion optics is based on a quadrupole mass filter which provides good mass separation and high transmission between sample surface and detector. However, to fully function as true mass filter in SIMS, where secondary ions are spread over a wide range of energies, the quadrupole filter has to be equipped with a prefilter energy analyzer to monochromatize ions for the mass filter. We presently test just such a setup in an independent experiment.

There the ion source of a UTI 100C quadrupole system is being replaced by a home-made, modified BALZERS ion optics in cylindrical mirror configuration. An alternate energy analyzer is being tested for comparison with this unit. It is based on a design commonly referred to as "Bessel Box"[3] and is

commercially available from Extranuclear Laboratories. Both analyzers provide a line-of-sight stop which effectively removes high-energy particles and photons from reaching the detector. The band-pass width for both analyzers were determined to be less than 1 eV by measuring thermally released impurity alkali ions from a heated tungsten filament.[9] During these tests both analyzers were found to exhibit some unwanted peculiarities: depending on specific energy transmission settings spurious ion signals are caused by, most likely, secondary ions desorbed from device walls. Such effects can be eliminated by choosing a more opportune energy window where such secondary effects do not exist. However, such a selection may necessitate a sacrifice of collection efficiency and corresponding loss in sensitivity. These preliminary tests have enabled us to develop an acute awareness of these trade-offs and will lead to a final solution once a real life test of the analyzers in conjunction with the Colcutron gun gets under way.

C. NF_x Source

The family of nitrogen based fluoride species identified by Ref. 1 as parts of transient laser discharges can most efficiently be derived from N_2F_4, tetrafluorohydrazine. At room temperature this gaseous compound is in equilibirum with relatively high concentrations of the difluoramino radical, NF_2.[10] This equilibrium can easily be forced in favor of NF_2 production by either multiphoton dissociation using IR laser[11] around 944 cm^{-1}, or by thermal dissociation of N_2F_4 through a heated nozzle. At nozzle temperatures of 500°K and pressures of 10^{-6} Torr total dissociation of N_2F_4 into NF_2 has been reported.[12] Since the highest dissociation yield for IR multiphoton dissociation is a mere 20%[11] thermal dissociation appears far more attractive.

Our design incorporates a passivated Ni nozzle which is resistively heated. Gas is fed into the nozzle by a needle-valve controlled foreline

which can be passivated, evacuated and purged independently from the sample chamber. This first design proved successful in dissociating N_2F_4, however, at an unacceptable price. The high temperature Ni releases significant amounts of impurities, from mass spectrometric data assumed to be S, which readily react with NF_2 thereby forming a highly undesirable form of molecular beam epitaxy on the sample surfaces which are to be studied in their reactions with NF_2. Presently, an alternative is being explored of replacing the Ni nozzle with a sapphire nozzle. No results are available from that source yet.

The radical NF which is expected to be more reactive than NF_2 has in the past more effectively been generated by scavaging one F atom from NF_2 with the aid of hydrogen or deuterium. Such a process proceeds via formation of a metastable HNF_2 (DNF_2) species[18] which then eliminates HF leaving the NF radical behind. For this process to occur a simple reactive flow system[13] has been shown to entirely suffice. Note, however, that for each NF one HF is generated and that H or D atoms are supplied in the flow system by the well-known reaction $H_2(D_2)+F \rightarrow HF(DF)+H$. On balance one therefore ends up with two HF's for each NF produced. Since it would be impossible to distinguish HF from NF caused effects by this method, the risk of observing minimal NF contributions against the well known wet etchant HF make a different approach mandatory. Collins and Husain[14] have photolyzed NF_2 by illuminating the strong absorption band at $\lambda = 2537$ Å, thereby receiving F and NF in an excited state. By passing the thermal molecular beam of NF_2 through the center of a double elliptical cavity, formerly used to pump a ruby laser, the photolysis method lent itself to easy adaption. The major problem in this approach turned out to be insufficient flux of 2537 Å photons from the laser flashlamps. The requirements posed by pumping a solid state laser differ from the present requirement in the low repetition rate and the spectral output which for ruby

and YAG lasers can be totally void of UV. Similarly to flash lamp pumped dye lasers, here a very fast risetime discharge is asked for. While the fast risetime prevents the laser dye from building up a significant portion of non-lasing triplet state population it also delivers a greater portion of the lamp's output in the UV part of the spectrum. The more rapid heating of the discharge plasma leads to higher instantaneous plasma temperature and therefore to a distinct blue shift overall. It was thus in our interest to modify the laser lamp control unit for higher repetition rate and faster pulse risetime. In the end, a whole new unit ahd to be built. This effort was a one semester project for one undergraduate student who was awarded the "1981 Hewlett-Packard Undergraduate Student Award" for his successful completion of the project. His paper showing the detailed circuitry is attached as Appendix A. The discharge lamp body which, especially for operation at higher pulse repetition rate (> 100 pps), has to be water-cooled is presently adapted to be used with a vacuum beam line instead of a laser rod.

RESULTS AND DATA ANALYSIS

Our etching studies on SiO_2 were preceded by equipment calibration experiments involving pure Si films on substrates identical with those that were later used for SiO_2. The 1000 Å films were evaporated by NWC and used in our experiments as received. All etching experiments were performed with the sample at room temperature with the exception of a few heat pulse experiments intended to reveal intermediate reaction products through thermal desorption. In these cases the sample was rapidly brought up to 100°C by forcing boiling water through the quartz crystal mount.

The kinetics of the XeF_2/Si system is by now well understood.[8] XeF_2 dissociates upon arrival of the Si surface whereby Xe desorbs instantly and

the adsorbed F undergoes different types of chemical interactions with Si ultimately forming SiF_2-like species. At room temperature these species are assumed to undergo a phase transition to SiF_4 at sufficient sample coverage. SiF_4 then desorbs into the gas phase and is being monitored mass-spectrometrically. On smooth Si films or Si single crystalline planes SiF_4 formation occurs therefore at room temperature once the F coverage exceeds a certain magnitude, perhaps about a monolayer.[8] Note, however, that comparison of such single crystal observations with optical coatings have to be attempted with great caution. Si films evaporated on silver-coated microbalance crystals by electron beam evaporation show not only polishing irregularities of the underlying substrate but a distinct morphology of their own. Figure 7 shows, for instance, a typical, "as-received" micron sized film structure of Si. It is only with reluctance that one would venture to extrapolate from single crystal XeF_2 etch yields, to explanations for the etch yield obtained from a sample as shown above. The quantitative features of our XeF_2/Si experiments have to therefore stand on their own and merely form the basis for comparison with approximately similarly structured silica films which were etched by the same method later on. We will return to a discussion of structural aspects after quantitative measurements have been presented. As described in the previous section "Experimental Facilities" quantitative etch measurements were performed by simultaneous microbalance and mass spectrometric observations.

The agreement between the two observations was determined to be not better than 50%. Such poor agreement is the result of several hard-to-guess quantities which enter the estimation of the mass spectroscopically found etch yield. First, there is a small yet significant permanent background of SiF_4 with or without a sample present in the chamber. Whatever the source of this background, passivation attempts as well as attempts to bake it away were

not successful. Since that background fluctuates, we were never quite able to identify whether or not the background scales linearly with ambient XeF_2 pressure. Secondly, the QMS source is located entirely out of sight of the reacting sample surface. Volatile SiF_4 molecules can reach its position only after one or, for the majority of desorption angles, multiple collisions with residual gas molecules or with the chamber walls. It is not known to what extent XeF_2 collisions with SiF_4 will reduce SiF_4 to SiF_3 and make it therefore appear as SiF_3^+ in the mass spectrometer. Nor is the pumping speed for these species known for either ion or cryopumps. Furthermore, SiF_3 may be governed by entirely different sticking probabilities than the volatile SiF_4 and may therefore get trapped at available surfaces without reaching th QMS ionizer. A conservative guess for all these intangibles leads to the above mentioned factor of discrepancy whereby the mass spectrometer always indicated the smaller reading. Next we will present the microbalance etch rate data for Si, SiO_2 Batch I and SiO_2 Batch II. All films were e-beam deposited on similar vendor-supplied (DETEC) silver coated quartz substrates. The etch rate data are those monitored by the microbalance while the XeF_2 flux is determined by summing the XeF^{++}, XeF^+, and XeF_2^+ mass spectrometer signals and thereby finding the XeF_2 partial pressure on an arbitrary scale. Note that the above mentioned discrepancies make an absolute calibration of the flow rate in terms of molecules per second, deduced from the mass spectrometer readings, somewhat questionable. We therefore plot in Fig. 5 the etch rate on Si against an arbitrary-units linear scale of XeF_2 partial pressure. We find a well reproducible linear relationship between XeF_2 ambinet pressure and etch rate, in good agreement with previous measurements.[8] However, our measurements consistently indicate a slope of less than 1 implying a slightly higher reaction probability for an otherwise identical[8] first order process. Whether

this disagreement is based on film structural aspects has not been clarified yet. In Fig. 6 we display the difference in etch rate between Si etched by XeF_2 alone and Si etched by ion-assisted XeF_2, i.e., without system backfill the ion gun was operated on the ambient residual gas at 400V anode voltage while XeF_2 was continuously reacting with the film. Due to the fixed spatial orientation of our system components it was impossible to carry out <u>in situ</u> an analysis of the true ion beam composition incident on the sample. Taking the fractionation ratios from our quadrupole mass analyzer ion source as a guideline, one has to expect the ion beam to comprise mostly XeF^{++}, XeF^{+}, and less than 15% XeF_2^{+}. With the composition of the bombarding beam loosely defined we find the etch rate increasing by about an order of magnitude from its value without the ion beam present. This increase is again somewhat larger than previously observed by Coburn and Winters[15] who observed an increase by a factor of 6 to 7 under Ar^{+} ion bombardment. The small discrepancy may be attributed to the mass difference of the incident ions in our experiment and the reactive nature of XeF versus the inert beam of Ar^{+} used in Ref. 15.

SiO_2 experiments with Batch I sample opened with a stunning surprise. Contrary to earlier claims[15,16] that SiO_2 remains unaffected by XeF_2 without additional stimulation by incident ions, photons or electrons, the Batch I films reacted so readily with XeF_2 that for the first couple of samples instrument malfunctioning was blamed for the unexpected "etch" behavior. However, Auger analysis of one unexposed sample and of several exposed Batch I samples showed relatively large C concentrations in the films or film residues. Such large C concentrations were not found in Batch II samples. Structurally, film residues of the C contaminated samples resemble a speckled surface with spots of silver shining bluish where the polycrystalline film had been removed.

The remaining crystals of Batch I were checked for consistency with the rest of Batch I without any intent of detailing the role which carbon plays as an impurity during the etching process. Since areas of the etched films appeared seemingly unetched under examination by optical microscopy local carbon aggregation, if carbon is indeed facilitsting etching, must have occurred during evaporation or handling and transport and would have made the issue not only one of bonding-state chemistry but also one of bonding site. Without preemptying our discussion on surface microscopy it should be noted here that future studies of optical film etching will have to concentrate on structural aspects with greater dedication than was considered prudent up to now. This is true also for films without major impurities.

Batch II SiO_2 films were immediately upon arrival Auger analyzed for evidence of impurities. None were found. Subsequent exposure to XeF_2 led to initial film building, as discussed for pure Si films, and no etching. This lack of chemical activity was confirmed by both the microbalance technique and the absence of above-noise signals for SiF_x ($x = 2,3,4$) in the residual gas spectrum.

A trial with fluorine atom etching (as opposed to XeF_2) did not show any measurable mass removal from the microbalance crystal and no visible chemiluminescence was observed. This is in contrast to recent published results of Si "gasification" by atomic fluorine.[17] Whether only the difference in F flux, the dissociation apparatus of Ref. 17 is operated at 1 Torr while the WSU device produces--without the added pulse-mode feature described in Section II "Experimental Facilities"--about 10^8 F atoms/cm^2 sec, or whether other differences are cause for this discrepancy is presently still under investigation.

When the XeF_2 flow rate is kept fixed so that the total system pressure is maintained at 5×10^{6} Torr and the ion gun is turned on without any further system backfill by Ar a very small ion current can be produced and made incident on the SiO_2 sample. Even at ion current levels of tens of nanoamps, i.e., well below the 0 - 1 μA dynamic range of the measuring instrument, etching of SiO_2 Batch II samples takes place while none had been observed without the ion beam. It is remarkable that etching proceeds at a rather rapid rate under that condition. At 400V ion energy the rate is 2×10^{-8} g/min, as determined by microbalance mass loss measurement, and is comparable with the etch rate found for pure Si films under similar conditions. A few data points exist showing a weak dependence of etch rate on incident ion energy but more data over a wider energy range will be required to firm up that conclusion. The etch rate enhancement can easily be documented by misdirecting the ion beam to cover only part of the sample surface and thereby creating an imbalance in film removal which can be noticed by bare eye after removal of the sample from the chamber (see discussion regarding Fig. 11).

Turning now to the structural features of film etching we note that our previous discussion had suffered from the problem of comparing single crystal or homogeneous film etching with results from highly structured films. We will now attempt to speculate on a relationship between that structure and observed etching. Since the program was initially not specifically aimed at this problem area the investigative tools were naturally limited in scope. We used optical microscopy during etching and, after gold coating (~150 Å) all dielectric films, scanning electron microscopy for comparison of etched and as-received samples. There is one major concern with high energy electrons of 20 keV interacting with dielectrics such as SiO_2. It is well known that Auger analysis using far lower energy electrons changes surface stoichiometry

in SiO_2 and that, in spite of a thin gold cover-film, alkali halide films structurally disintegrate under scanning electron beam bombardment. We have not investigated to what extent the present samples are subject to similar structural modifications during analysis. We are, however, convinced that any such effect cannot satisfactorily explain observed differences between etched and unetched surfaces. We presently attempt to eliminate any uncertainty in this regard by carbon replicating sample surfaces without losing essential resolution. All pictures shown in the following were taken of original, unreplicated surfaces.

In Fig. 7 we present a 2000X magnified, as-received Si film that clearly shows the wide variety of features and characteristic scale length structures which make apparent the aforementioned problem of assuming single crystal behavior. We have not investigated a film-free quartz crystal surface for comparison but presume that a film of not more than 1000 Å thickness will generally follow the underlying substrate structure even if nucleation proceeds unevenly across the surface (and may thus account for some of the observed structure). For comparison we next show a SiO_2 Batch I film in its unetched (Fig. 8a) and etched (Fig. 8b) topography. The unetched films show no signficant change in morphology from the one observed in pure Si films and are mostly following the underlying substrate structure as above. After etching, however, the original average micron size scale structure is found to have turned into globular features which consist overwhelmingly of SiO_2 with C as only major impurity (as measured by Auger analysis). A larger surface area than in Fig. 8b is shown in Fig. 9 where the wide spread in globular size distribution becomes more apparent. We have not yet investigated the possible mechanisms for the formation of spherical globules under the influence of an etchant. One suggested hypothesis speculates that the

silicon-oxygen stoichiometry changes from SiO_2 to SiO_x around the edges of scales similarly to grain boundary chemistry effects of polycrystalline bulk materials. The change in stoichiometry is accompanied by the appearance of unsaturated bonds or dangling bonds which offer readily available adsorption states for the etchant to latch on to. Furthermore, defect states associated with dislocations or edges will act similarly, directing the etch process to proceed from the scale edges inwardly. Why the spherical globules attain their significant shape as their final, energetically preferable form is not known, nor is it certain that they maintain long range order throughout. It is conceivable that they become glassy, if not throughout, then at least around their surface. We have refrained from analyzing this problem so far for two reasons.

Although similar etching topographies were found in Batch II samples and cannot be disregarded merely as impurity caused aberrations, no results are available for etch topographies by agents other than XeF_2. The globules are not yet a common feature of SiO_2 films etched by any other fluorinated agent.

Second, globules are found to extend over a size range from 0.1 to 1.0 microns. Crystallographic analysis of dielectric particles of that size requires tools of formidable complexity which none of the investigators on this contract has presently available. There was a great deal of reluctance about entering into difficult experiments which later may prove to be of only marginal importance, if no globules are found for other etchants.

As was pointed out before, Batch II SiO_2 films did not contain C impurities or any other noticeable impurities. Nevertheless, globular etch morphology was also found there. In Fig. 10a an unetched surface is compared with an etched surface (Fig. 10b) exposed to XeF_2 only and an etched surface

(Fig. 10c) which was simultaneously treated by ion bombardment and XeF_2. The ion energy was 400V. The images of Fig. 10 represent each a different crystal surface. While Batch I samples turned into densely covered globule fields Fig. 10b clearly shows a mere onset of globule formation in Batch II samples under similar conditions. With additional ion impact the combined effect of physical and chemical sputtering lead to formation of globular clusters of smaller sized globules. The average globule size is reduced to greatly less than 1 μm. Again, the detailed mechanism for this effect is presently not understood.

Finally, in Fig. 11 we present the case of a Batch II SiO_2 film which was only partially covered by the ion beam. Aside from the clearly noticeable demarcation line between ion exposed and unexposed areas down the middle of the picture we note the lack of striation in the underlying silver film structure which was a dominant feature in Fig. 10c. In this case also the globules aggregate less and are of larger average size than in the comparison case. On the other hand, the unexposed areas in Fig. 11, left of the demarcation line, and in Fig. 10b resembly closely identical conditions. We are not yet prepared to identify the reasons for the obvious differences in morphology in the ion bombarded zones. All experimental parameters governing exposure in Fig. 10c and Fig. 11 were kept constant.

At this point in the experiment we can summarize our findings as follows:

i) E-beam evaporated SiO_2 films become much more susceptible to lasing medium erosion with impurities present in the film, as substantiated for C.

ii) Impurity-free SiO_2 films, prepared as for point i), etch barely when exposed to XeF_2 only and etch not at all when interacting with atomic F. The latter finding is, however, highly tentative at this time.

iii) Additional ion bombardment at relatively low ion energies (<100 μA) greatly enhances the etch rate on clean SiO_2 films.

iv) Temperature effects due to substrate temperature between room temperature and 100°C are insignificant.

FY 81 PROGRAM

In addition to the continuation of SiO_2 studies, quantitative studies will get under way involving MgF_2 and possibly cryolite and Al_2O_3. These films will again be analyzed by the crystal microbalance technique and Auger spectroscopy. However, more work will have to be done on determining the structural properties of films and relating these to the survival of films under XeF_2, F, and NF_x attack. It has become evident during the first phase of this work that the maximum pay-off for this program will not be achieved without a thorough analysis of this relation. To that end, optical-quality surface quartz crystals will be employed as microbalance deposition substrates. SiO_2 film surface roughness features which so far had to be attributed to the underlying substrate will thus be eliminated. Different deposition techniques are presently under discussion and will be tried as far as the financial and manpower framework of this program permit.

Certain steps in the reaction kinetics of XeF_2 with SiO_2 which have so far remained without explanation, i.e. the early phase mass deposition problem discussed above, will be approached by SIMS. Completion of this experimental facility has therefore acquired top priority.

Eventually, multilayer structures and the importance of certain film impurities will have to be investigated--multilayer structures for their obvious practical significance and impurities for providing chemical stability criteria which permit establishment of purity standards for coating materials.

Studies of synergistic effects will continue to play a crucial role. Etch rates by XeF_2, F, and NF_x will be determined as function of current density of concurrent incident electron or ion currents. Similarly, effects of 354 nm tripled Nd^{3+}:YAG radiation on etch rates will be analyzed.

REFERENCES

1. W. Chow, M. Stuke, and F. P. Schafer, Appl. Phys. 13, 1 (1977).

2. PCR Corporation, private communication.

3. C. J. Ultee, Chem. Phys. Lett. 46, 366 (1977);
   I. B. Goldberg and G. R. Schneider, J. Chem. Phys. 65, 147 (1976).

4. H. L. Chen, R. E. Center, D. W. Trainor, and W. I. Fyfe, Appl. Phys. Lett. 30, 99 (1977);
   B. I. Schneider and C. A. Brau, Appl. Phys. Lett. 33, 569 (1978).

5. D. E. Rosner and H. D. Allendorf, J. Phys. Chem. 75, 308 (1971).

6. D. E. Rosner and J. P. Starkey, J. Phys. Chem. 77, 690 (1973).

7. Dr. Ben Rosenblum, Bendix Corporation, Kansas City Division, Kansas City, Missouri 64141.

8. H. F. Winters and J. W. Coburn, Appl. Phys. Lett. 34, 70 (1979);
   T. J. Chuang, J. Appl. Phys. 51, 2614 (1980).

9. J. H. Craig and J. L. Hock, J. Vac. Sci. Technol. 17, 1360 (1980).

10. F. A. Johnson and C. B. Colburn, J. Amer. Chem. Soc. 83, 3043 (1961).

11. A. S. Sudbo, P. A. Schulz, E. R. Grant, Y. R. Shen, and Y. T. Lee, J. Chem. Phys. 70, 912 (1979).

12. S. N. Foner and R. L. Hudson, J. Chem. Phys. 58, 581 (1973).

13. J. M. Herbelin, D. J. Spencer, and M. A. Kwok, J. Appl. Phys. 48, 3050 (1977).

14. R. J. Collins and D. Husain, J. Photochem. 2, 459 (1973).

15. J. W. Coburn and H. F. Winters, J. Appl. Phys. 50, 3189 (1979).

16. J. W. Coburn and H. F. Winters, J. Vac. Sci. Technol. 16, 391 (1979).

17. V. M. Donnelly and D. L. Flamm, J. Appl. Phys. 51, 5273 (1980).

FIGURE CAPTIONS

Figure 1 a) Block diagram of the discharge RF oscillator pulser. The switching stages are floating and are actuated by optocoupler elements.

b) and c) Circuit diagram of one isolated optical switch with floating supply.

Figure 2 Circuit diagram of ion source filament current interrupt device. To isolate the control transistors from ground their base bias is adjusted by a TIL 112 optocoupler.

Figure 3 Schematic of the turbopump control circuit.

1 = ALCATEL mechanical forepump
2 = Forepump control relay
3 = Common circuit breaker for forepump and turbopump
4 = Turbopump circuit breaker (8A)
5 = Turbopump motor
6 = Turbopump control relay
7 = Valve control
8 = Cooling water flow switch
9 = Heater control relay
10 = Heater
11 = 110V to isolation transformer
12 = Manual heater switch

Figure 4 Cross sectional drawing through alumina RF discharge vessel. The Macon ceramic insert originally used has since been replaced by an alumina piece with a 1/16" channel terminating into a 0.006" orifice.

Figure 5 Typical XeF_2 caused etch rate from SiO_2 versus XeF_2 partial pressure. The etch rate is measured by a quartz crystal microbalance. For comparison etch rate data from Ref. 8 following a slope of 1 are added.

Figure 6 Comparison of ion enhanced and pure XeF_2 etch rates on 1000 Å Si films versus XeF_2 partial pressure.

Figure 7 Morphology of 1000 Å e-beam evaporated Si film (magnification 2000 X).

Figure 8 a) As-received 1000 Å SiO_2 Batch I film at 5000 X magnification.

b) Batch I SiO_2 film after exposure to pure XeF_2. Note spread in size distribution among SiO_2 globules.

Figure 9 Same surface as in Fig. 8b at 5000 X magnification.

Figure 10 a) 1000 Å SiO_2 Batch II film as-received. No signficant structural properties different from Batch I films as shown in Fig. 8a.

b) 2000 X magnification of SiO_2 Batch II film after exposure to XeF_2. A mere onset of globule formation is observable.

c) Similar Batch II SiO_2 film as in Fig. 10b but after concurrent etching by XeF_2 and low energy (400 eV) ion beam.

Figure 11 2000 X magnified Batch II SiO_2 film surface after full surface exposure to XeF_2 and partial (right half of picture) exposure to ion beam of 400 eV.

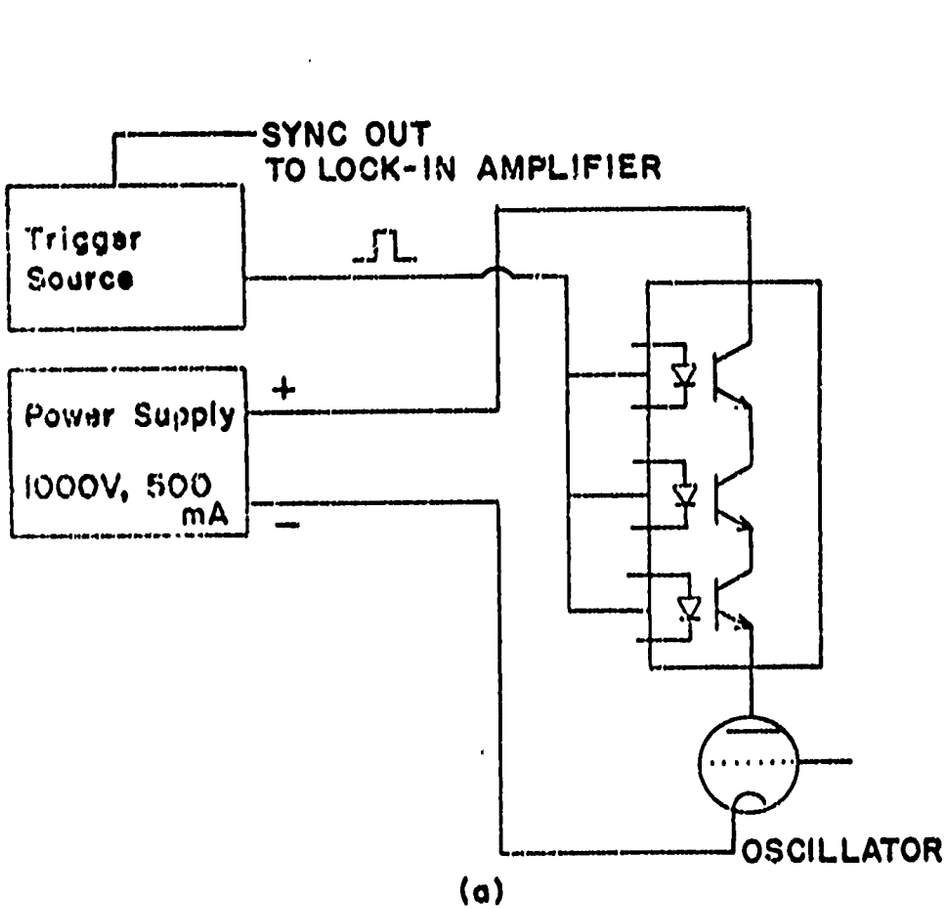
SYNC OUT
TO LOCK-IN AMPLIFIER
Trigger Source
Power Supply
1000V, 500 mA
+
−
OSCILLATOR

(a)

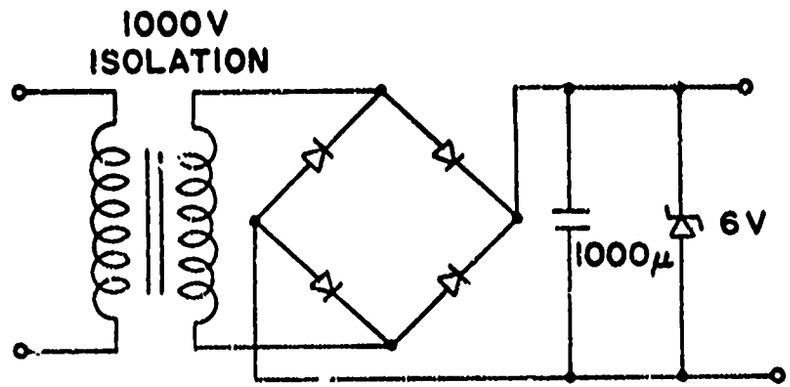
1000V
ISOLATION
1000μ
6V

(b)

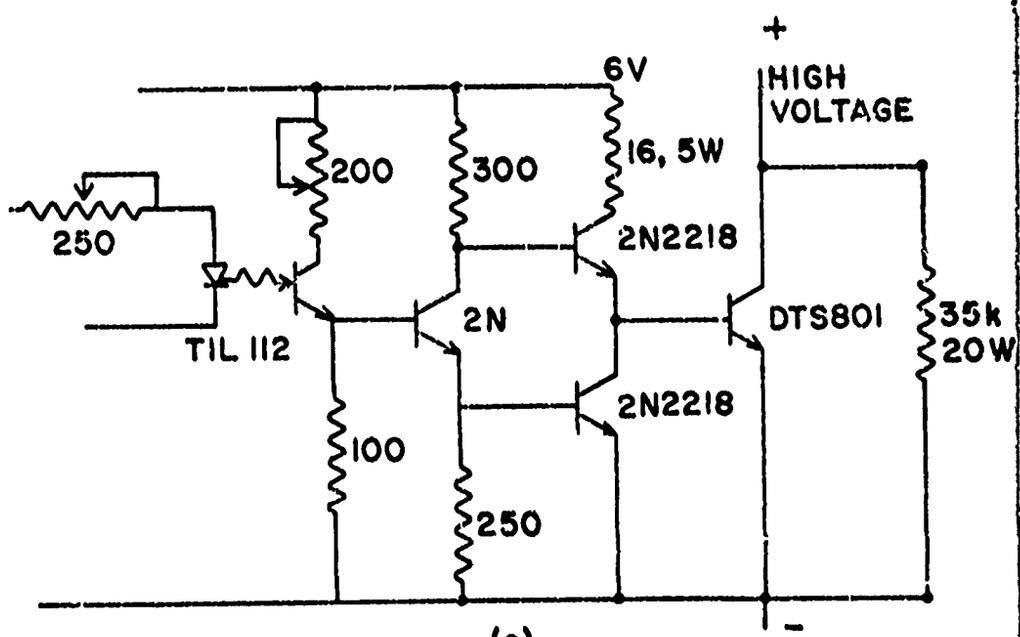
+
6V
HIGH VOLTAGE
200
300
16, 5W
250
2N2218
2N
DTS801
35k 20W
TIL 112
2N2218
100
250
−

(c)

Fig. 1

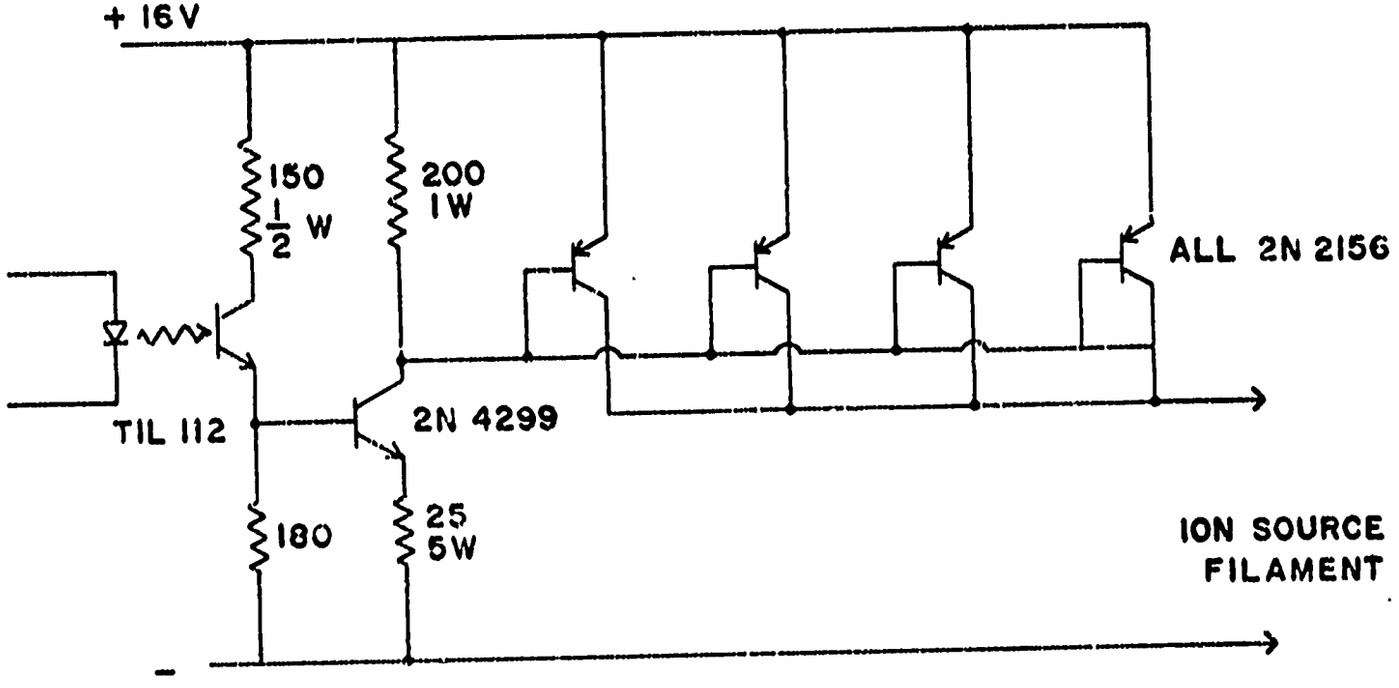
+ 16V
150
1/2 W
200
1W
ALL 2N 2156
TIL 112
2N 4299
180
25
5W
ION SOURCE
FILAMENT
-

Fig. 2

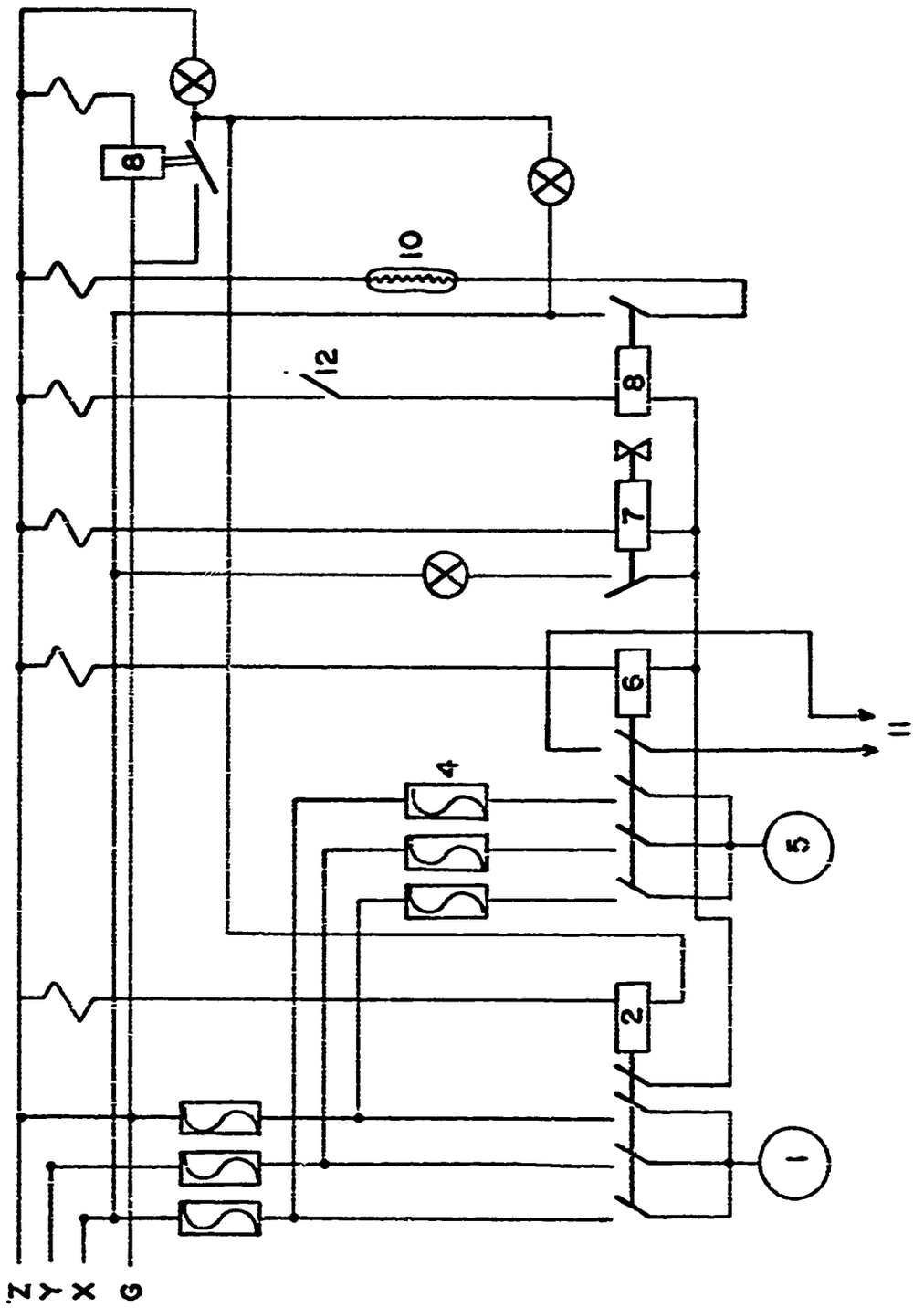

Fig. 3

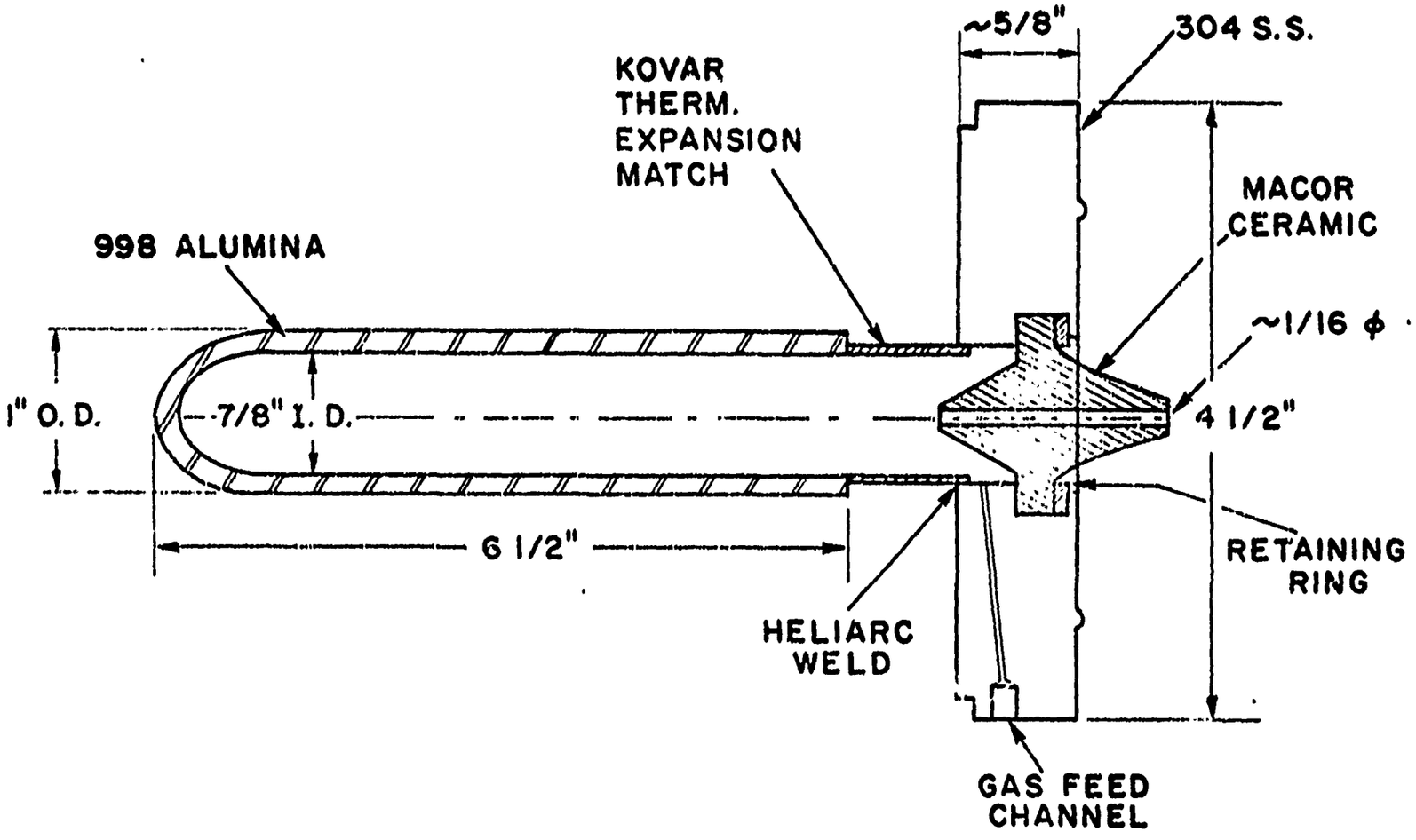
~5/8"
304 S.S.
KOVAR
THERM.
EXPANSION
MATCH
MACOR
CERAMIC
998 ALUMINA
~1/16 ϕ
1" O. D.
7/8" I. D.
4 1/2"
6 1/2"
RETAINING
RING
HELIARC
WELD
GAS FEED
CHANNEL

Fig. 4

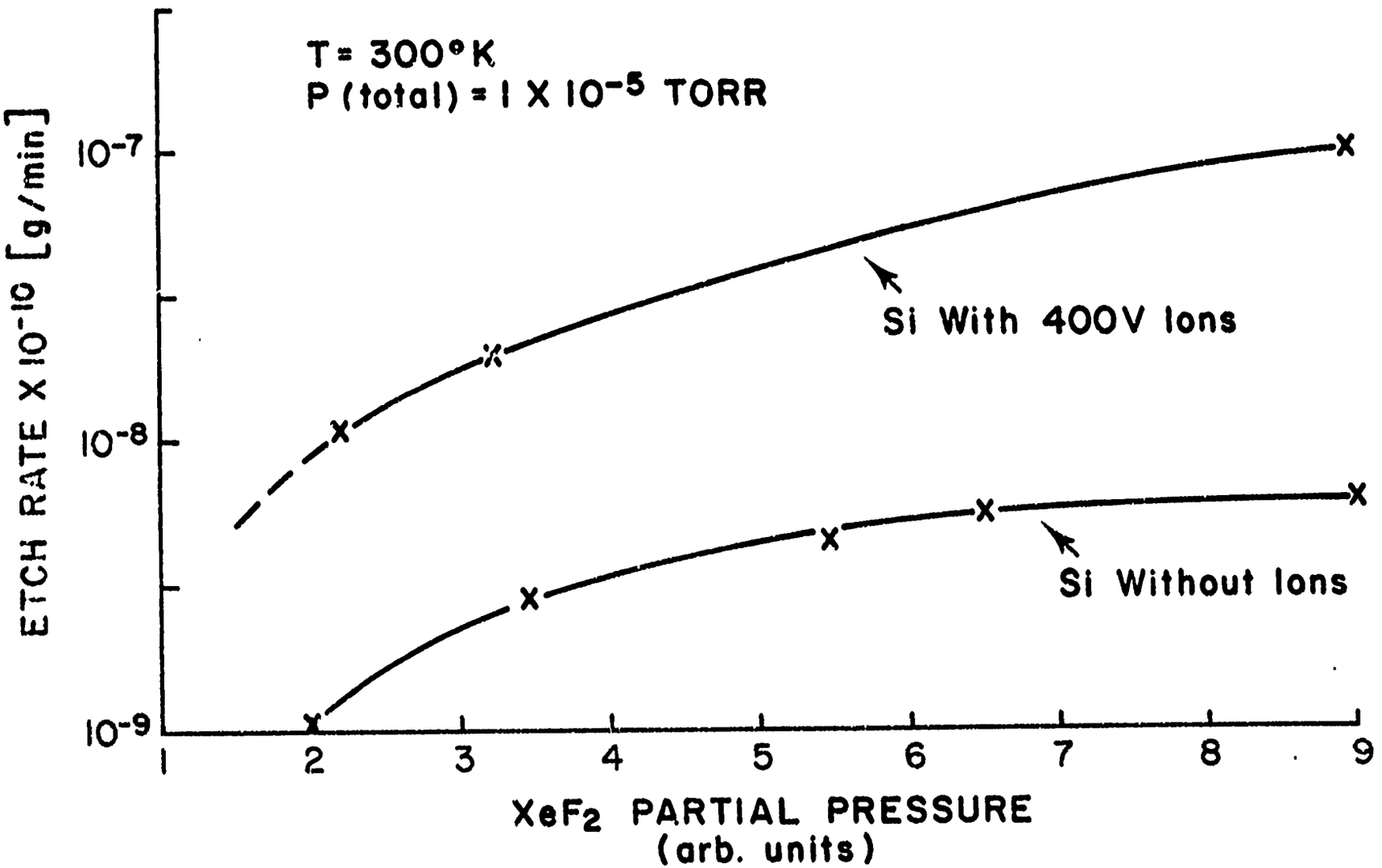
T = 300°K
P (total) = 1 X 10⁻⁵ TORR
ETCH RATE X 10⁻¹⁰ [g/min]
10⁻⁷
10⁻⁸
10⁻⁹
Si With 400V Ions
Si Without Ions
1
2
3
4
5
6
7
8
9
XeF₂ PARTIAL PRESSURE
(arb. units)

FIG. 5

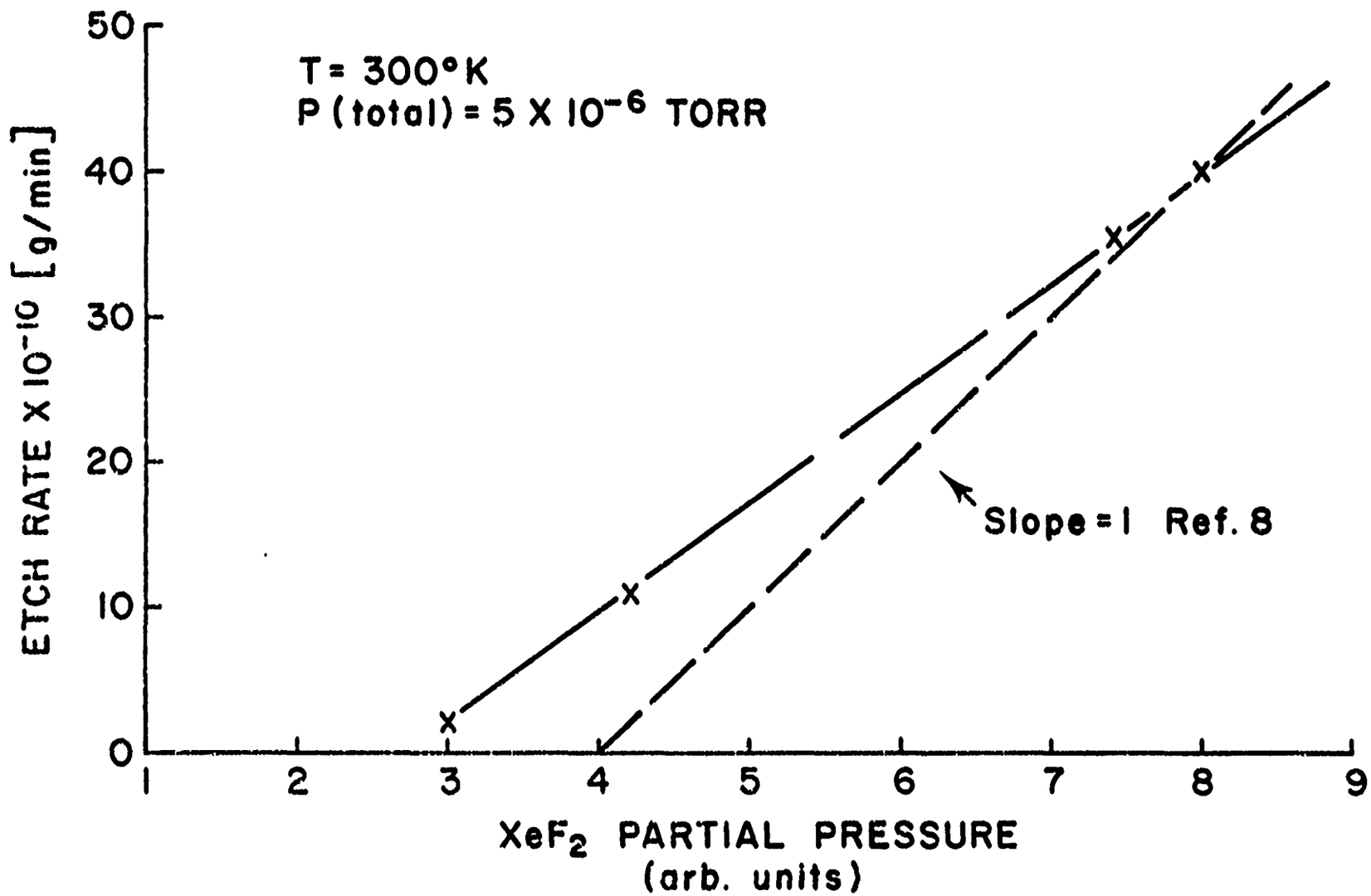
T = 300°K
P (total) = 5 X 10⁻⁶ TORR
ETCH RATE X 10⁻¹⁰ [g/min]
50
40
30
20
10
0
1
2
3
4
5
6
7
8
9
Slope = 1 Ref. 8
XeF₂ PARTIAL PRESSURE
(arb. units)

Fig. 6

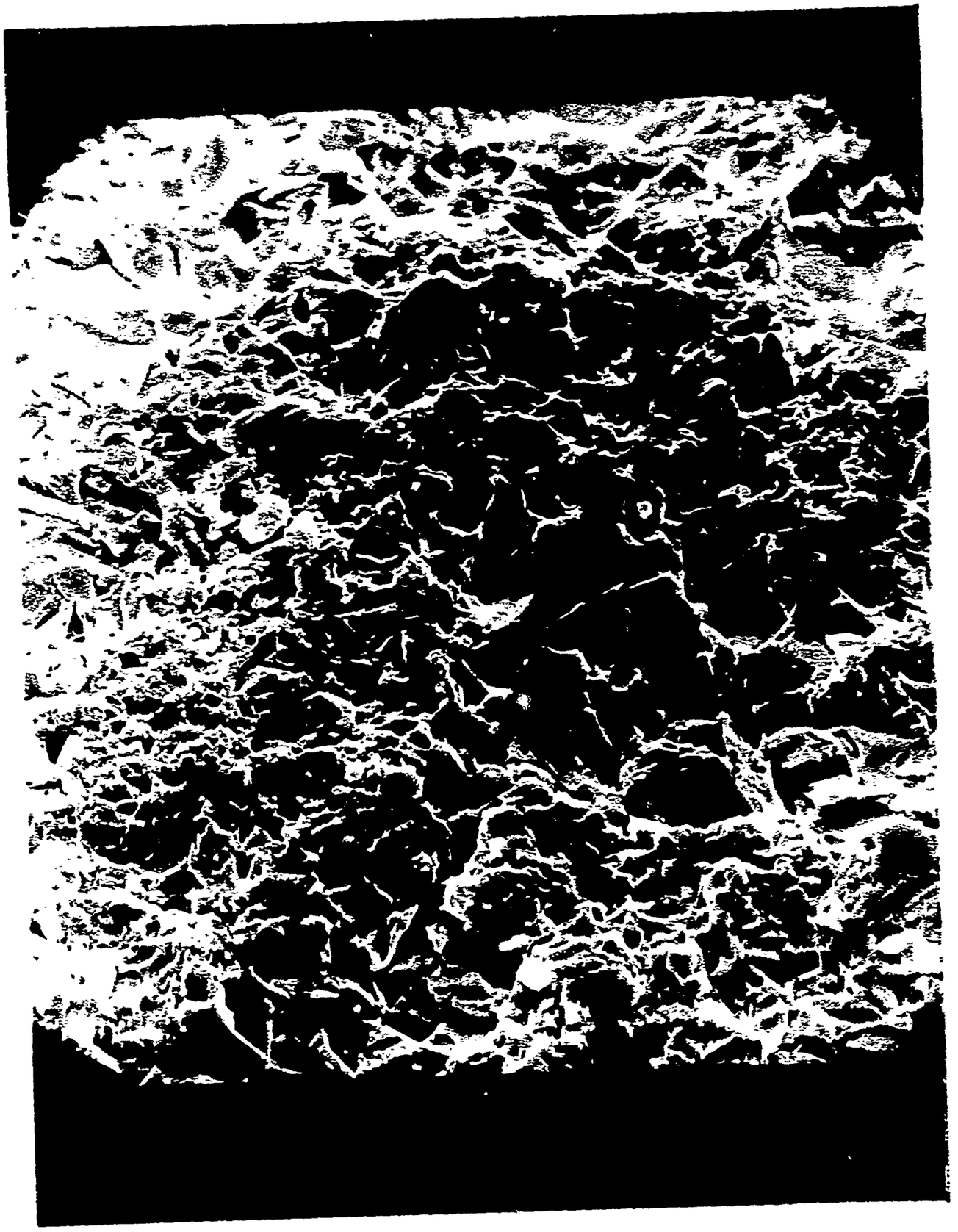

Fig. 7

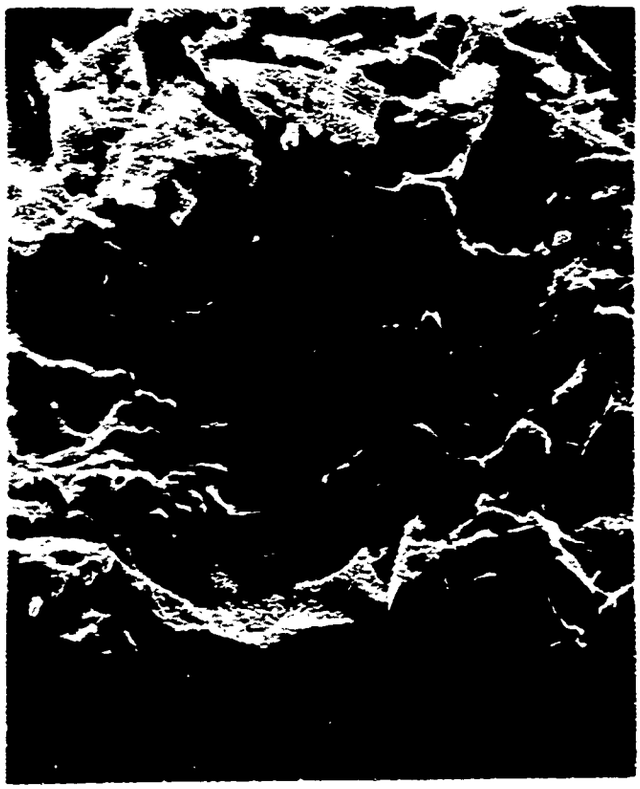

8A 8B

Fig. 9

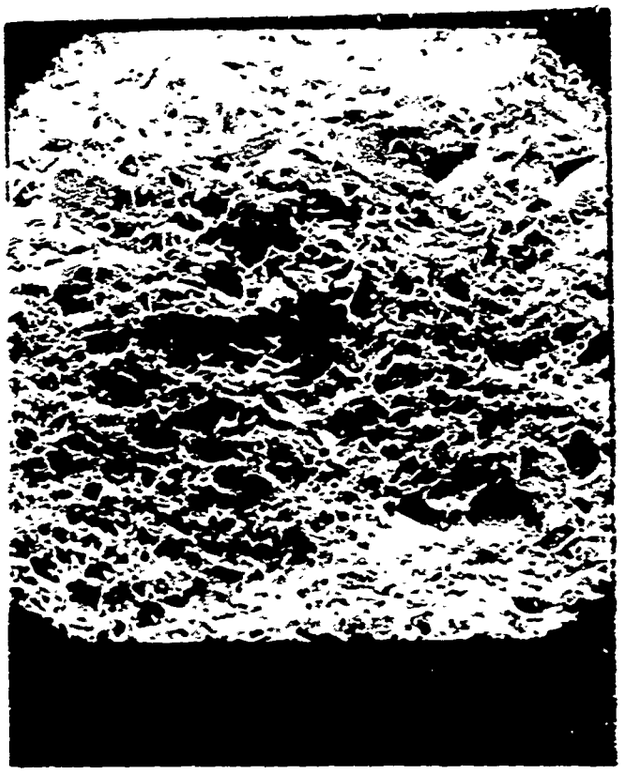

10 a)

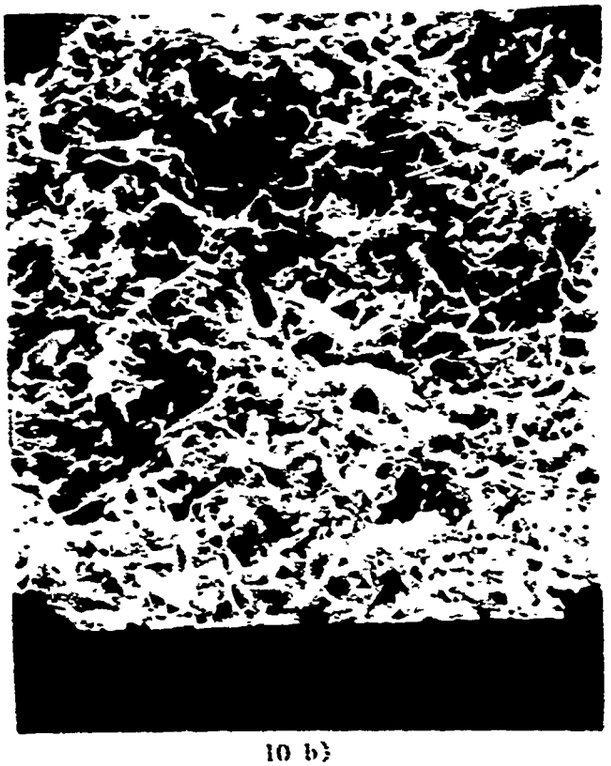

10 b)

10 c)

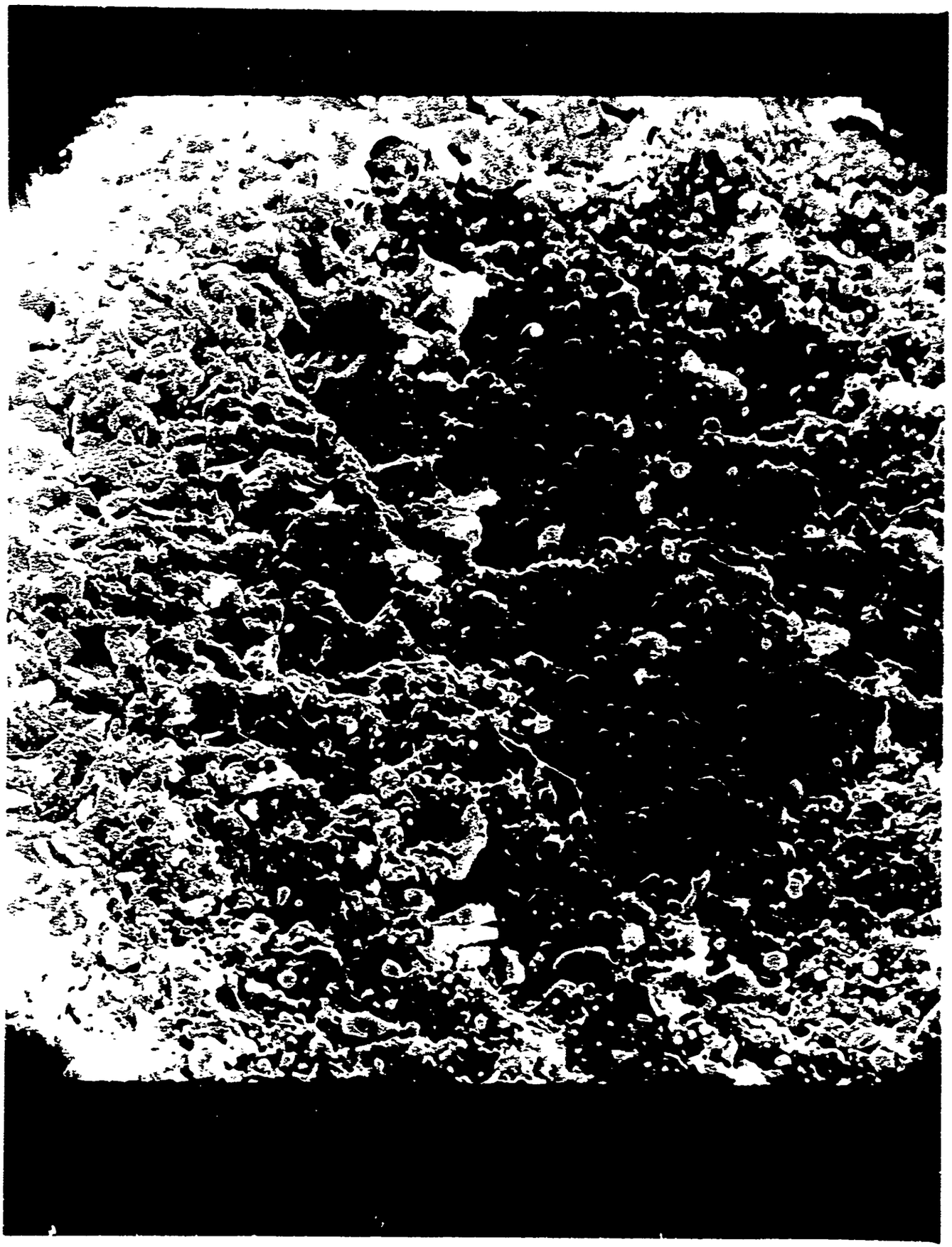

Fig. 13

Appendix A

A HIGH RISE TIME FLASHLAMP DISCHARGE CIRCUIT

Rob Townsley
Washington State University

Introduction:

Efficient operation of flashlamps is crucial in many scientific and technological efforts. Currently, the most prominent applications of flashlamps are in flashlamp pumped, pulsed solid and liquid lasers, in photochemical technology such as the curing of resins and in pulsed warning beacons for navigation. Obviously, different applications require different flashlamps and different operating conditions for optimum performance in such devices.

In the case of photolytic dissociation of molecules or pumping of solid state or liquid lasers, the flashlamp functions to provide sufficient photon flux in that part of the spectrum which is most readily absorbed by the molecule of interest or lasing ion. The corresponding absorption bands or lines are usually fairly narrow, making the flashlamp with its broadband blackbody output a poorly tuned source. In order to enhance flashlamp emission into respective fixed absorption bands, one may choose a proper flashlamp gas which, when suitably ignited, will emit a strong characteristic spectrum in addition to the smooth blackbody output. Choice of the gas will be dictated by the match between characteristic emission lines and the test molecule's absorption bands.

Very often flashlamp pulses are also required to provide fast risetimes. Commonly these risetimes are of the order of 10^{-6}s. If shorter risetimes are mandated by the particular application,

a well designed discharge circuit for the lamp must minimize the inductance in all circuit components. In the ultimate design, the flashlamp itself is the principle inductive element.

The purpose of the effort described here is development of a fast discharge circuit for photodissociation of halogen bearing molecules and investigation of effects caused by the chemical radicals resulting from the dissociation. The overall effort is still in progress and this report focusses only on the hardware development.

Suggested Solution:

During a regular discharge the self-inductance of the lamp is initially high because of a small current filament (also referred to as a streamer) along the bore of the lamp which develops first. This large initial inductance can be reduced by continually simmering the lamp and slowly prepulsing before the larger portion of discharge energy is applied. The effect of the prepulse is to facilitate a controlled reduction in lamp self-inductance. As long as the pulse repitition rate on the lamp is low, the minimum in self-inductance will be achieved at a certain, experimentally determined (for each particular lamp), enhanced simmer or prepulse current level. If the main discharge is initiated at precisely the time this minimum in self-inductance is reached, the risetime on the main discharge will steepen. In addition, the light output of the lamp will increase not only in total, but primarily in the characteristic portion of the spectrum. The latter will predominantly act as

stimulus in the desired photodissociation.

Experimental Approach:

The flashlamp employed in the Washington State University apparatus are commercially available, Xenon filled, water-cooled lamps of three inch arc length and 4 mm bore diameter. Since the lamp drive circuit has to provide three functions--continuous simmer, enhanced simmer, and main discharge--the circuit parts responsible for these functions will be described separately. Two lamps will ultimately be operated in series at a maximum energy dissipation of 10 J per pulse per lamp. All circuit parts have therefore been chosen with this specification in mind.

A further, economical constraint on the design limited the DC power supplies for execution of the three previously mentioned functions to only one supply. This supply has a current-stabilized continuously variable voltage output of 0-2000 V with currents up to 1500 mA over the whole voltage range.

A generalized block diagram in Fig. 1 shows the separate power switching modules connected to the single power supply.

1) Continuous Simmer:

A gas discharge is a non-ohmic load. The voltage drop across one of the lamps in the WSU circuit was found to be less than 250 V at 100 mA current and around 300 V at 50 mA, with both measurements done in the same ignite-squelch cycle. It was also found that below 30 mA the ionization in the lamp remains nonself-sustaining. In determining the optimum DC simmer

current, one has to decide between the trade-offs of high enough current to maintain continuous simmer operation and low current to reduce electrode sputtering and increase lamp lifetime. A current of 50 mA was chosen. It is provided by the 2 kV power supply through a pair of wire-wound ballast resistors totalling 25 kΩ. A high voltage diode (MR 250-5) is used to suppress high voltage ringing from reaching the power supply if improper discharge should occur.

Before any continuous simmer current can be established through the lamp, an initial ionizing event must be generated. Usually a three inch bore length Xe lamp does not break down if a mere 2000 V is applied across the electrodes. A field-ionizing pulse of several times higher voltage has become the customary procedure in initiating discharge in such lamps under these conditions. Such a pulse is usually (and in the device described here) generated through a low inductance, high voltage trigger transformer. In accordance with lamp manufacturer's specifications, a so-called series-injection trigger configuration was chosen. In this mode the trigger transformer secondary side is an integral part of the discharge circuit as shown in Fig. 2. The main advantage of this triggering mode lies in the lower trigger voltages required and thus in the diminished danger of spurious high voltage pulses leaking into and destroying components in other discharge unit modules.

The trigger transformer primary side is fired manually from the flash unit front panel control.

2) Simmer Current Enhancement:

In Fig. 3 the control of the simmer current enhancement by a SCR (50 RAI 120) circuit is shown. Since high forward voltage, fast risetime, economical SCR's are just becoming available, a design could be followed which uses two 1000 V SCR's in series. Both SCR's are being triggered with negligible jitter by the same external source. To isolate the trigger source from the high voltage section a double secondary 1:1:1 trigger transformer is employed. A simple resistive voltage devider assures a voltage balance across each SCR as a protective measure. In the same vein, a group of fast turn-on Zener diodes (IN 5113) together with (IN 4249) rectifier diodes protect each SCR gating circuit from overvoltage and reverse bias pulses. Unfortunately, the benefit of protection by the transformer comes at the expense of an additional power supply required to provide sufficient pulse power for the transformer primary side. An operating voltage of 60 V in that current was found sufficient for reliable trigger operation. As an additional protection, the external trigger source is entirely decoupled from the whole discharge control unit by a TIL 112 optocoupler. Prototype testing clearly indicates that such protective measures are recommended.

3) Main Discharge Circuit:

After the enhanced-simmer SCR's turn on, the current in the flashlamp increases from 50 mA to 3 A in slightly less than 100 μs. At the high simmer current, the current filament is assumed to fill the entire bore of the lamp. The slow risetime

is set by the presence of the inductor. It not only allows for a steady reduction in lamp self-inductance but for sufficient switching time in all components of the main discharge trigger circuit.

As main discharge switching element a fast risetime, hydrogen filled thyratron (EEV CX 1571) is employed. The tube bias circuit is shown in Fig.4. Since the on-state resistance of the tube is significantly smaller than that of the series-pair SCR's, the tube, once it is turned on, essentially shunts the enhanced simmer.

The enhanced simmer current is driven through a 1 Ω, 25 W sensing resistor, the voltage drop across which is probed by a 1% Zener diode. As soon as the enhanced simmer current exceeds 2.8 A the Zener diode turns on, thus bringing the photocoupler TIL 112 to the on state. As shown in Fig. 5, this sequence results in discharging the RC network through the trigger transformer TR131 which, in turn, applies a gating pulse to the thyratron.

Present Project Status:

The project is presently still incomplete. However, all hardware elements have been built and modified in accordance with improvements mandated by breadboard tests. The entire continuous simmer module, the simmer initiation module, and the simmer enhance module are operating reliably. Debugging efforts presently concentrate on the thyratron trigger module where low voltage leakage and high voltage flashover problems have been encountered. Further improvements in this module will be forthcoming.

FIGURE CAPTIONS:

Fig. 1: Schematic discharge block diagram of modular approach to problem.

Fig. 2: Circuit diagram of initial continuous simmer initiation module.

Fig. 3: Circuit diagram of SCR controlled enhanced simmer module.

Fig. 4: Circuit diagram of thyratron bias network.

Fig. 5: Circuit diagram of thyratron gate trigger circuit in main discharge module.

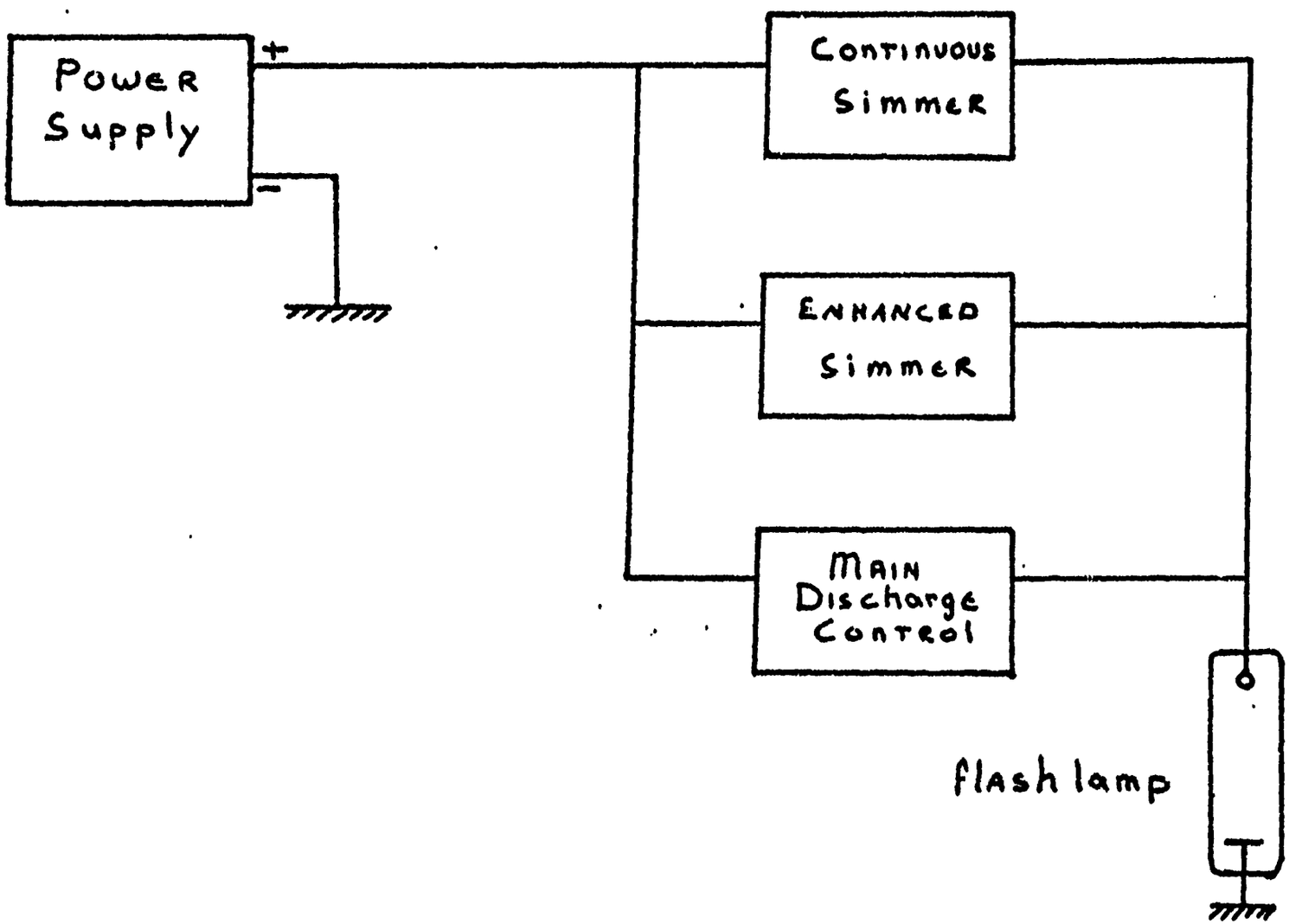
Power Supply
+
−
Continuous Simmer
Enhanced Simmer
Main Discharge Control
flash lamp

Fig. 1

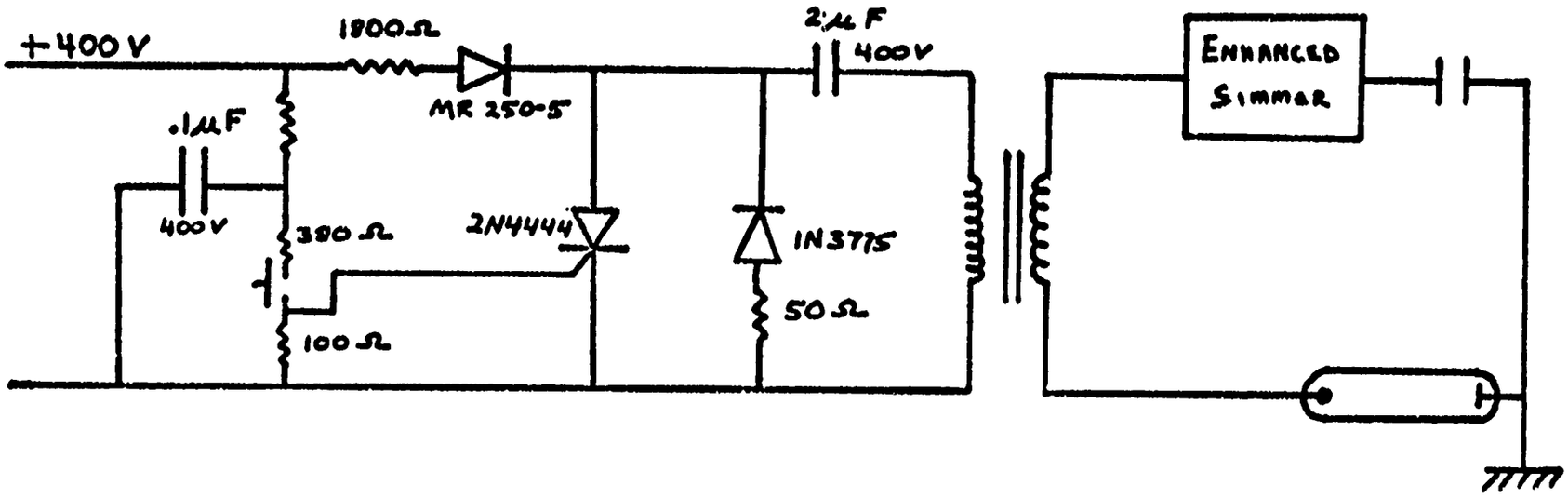
+400 V
1800 Ω
MR 250-5
2 μF
400 V
.1 μF
400 V
390 Ω
2N4444
1N3715
50 Ω
100 Ω
ENHANCED
SIMMER

Fig. 2

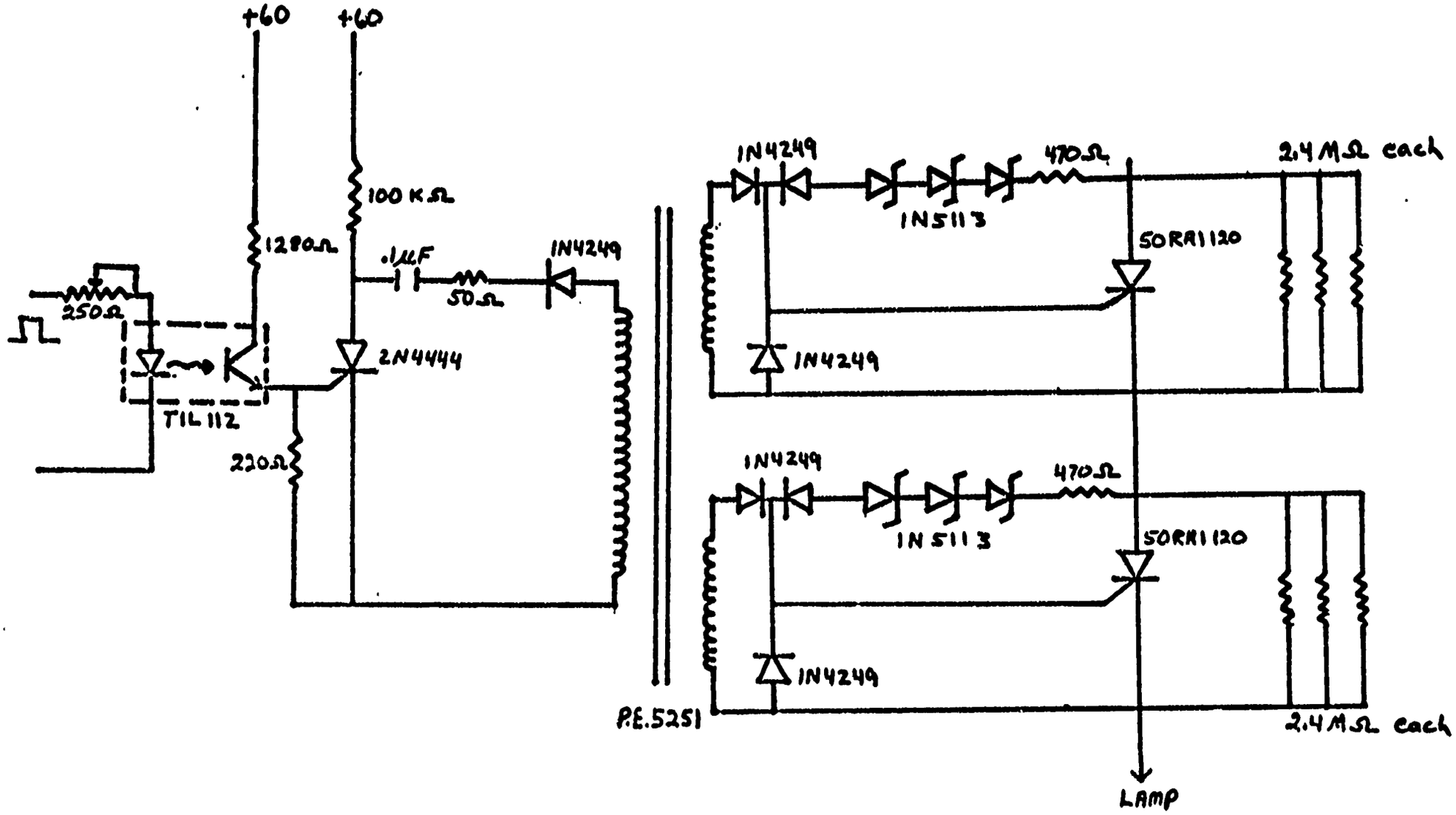
+60
+60
100 KΩ
1280Ω
.1μF
50Ω
IN4249
250Ω
2N4444
TIL 112
220Ω
P.E.5251
IN4249
470Ω
2.4 MΩ each
IN5113
S0RA1120
IN4249
IN4249
470Ω
IN5113
S0RA1120
IN4249
2.4 MΩ each
LAMP

Fig. 3

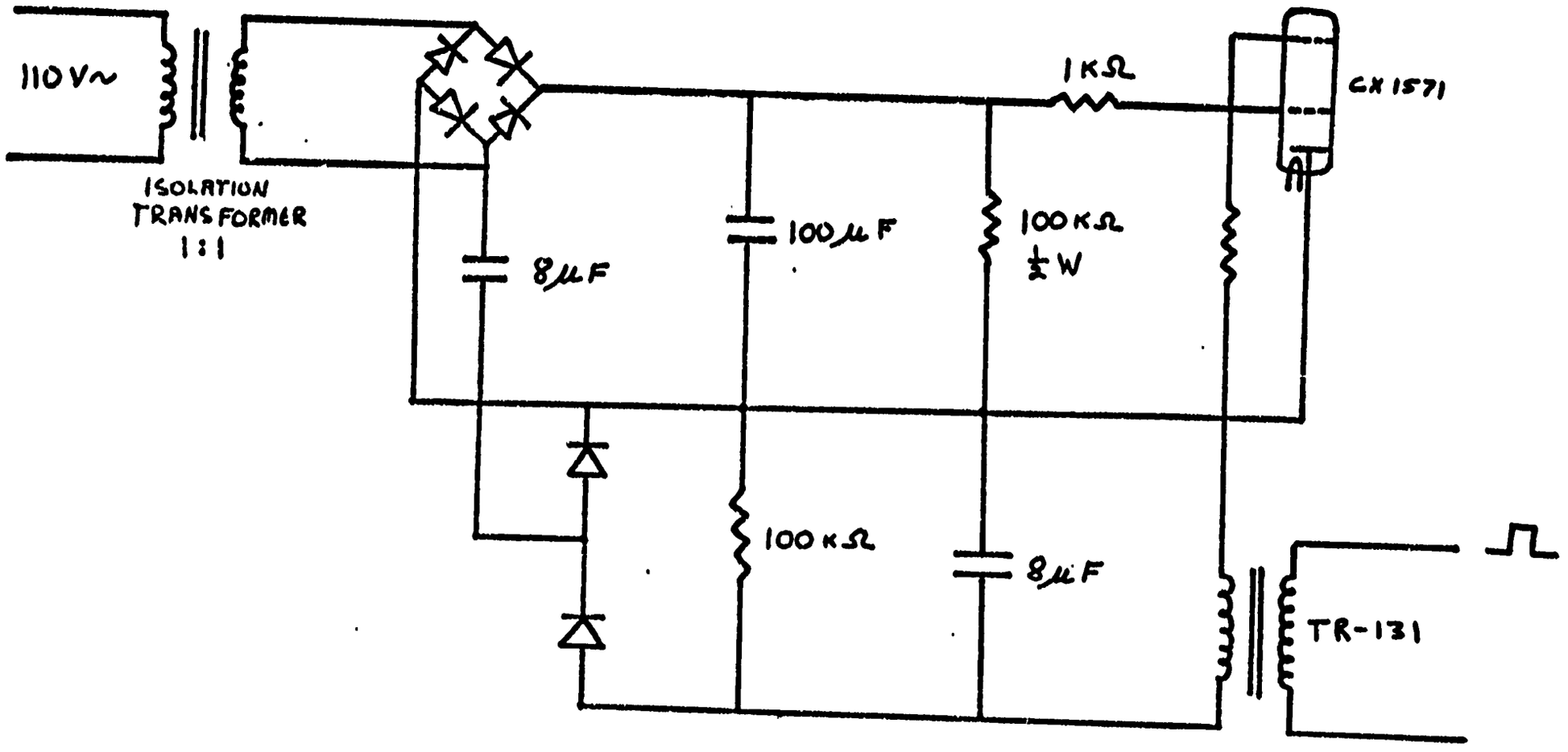
110V~
ISOLATION
TRANSFORMER
1:1
8μF
100μF
1KΩ
100KΩ
±W
CX1571
100KΩ
8μF
TR-131

Fig. 4

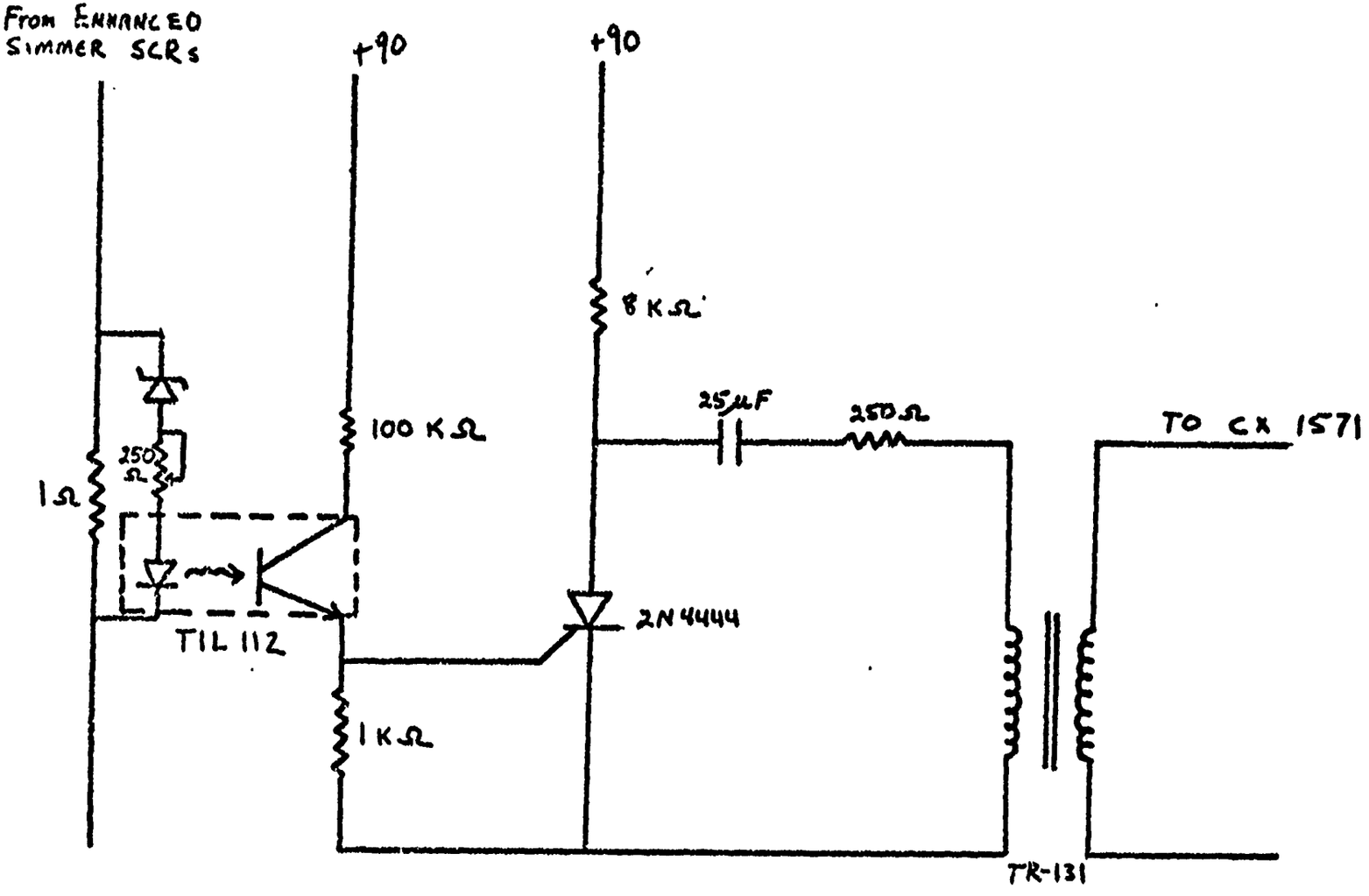
From Enhanced
Simmer SCRs
+90
+90
8 KΩ
25μF
250Ω
TO CX 1571
100 KΩ
250
Ω
1Ω
TIL 112
2N4444
1 KΩ
TR-131

Fig. 5

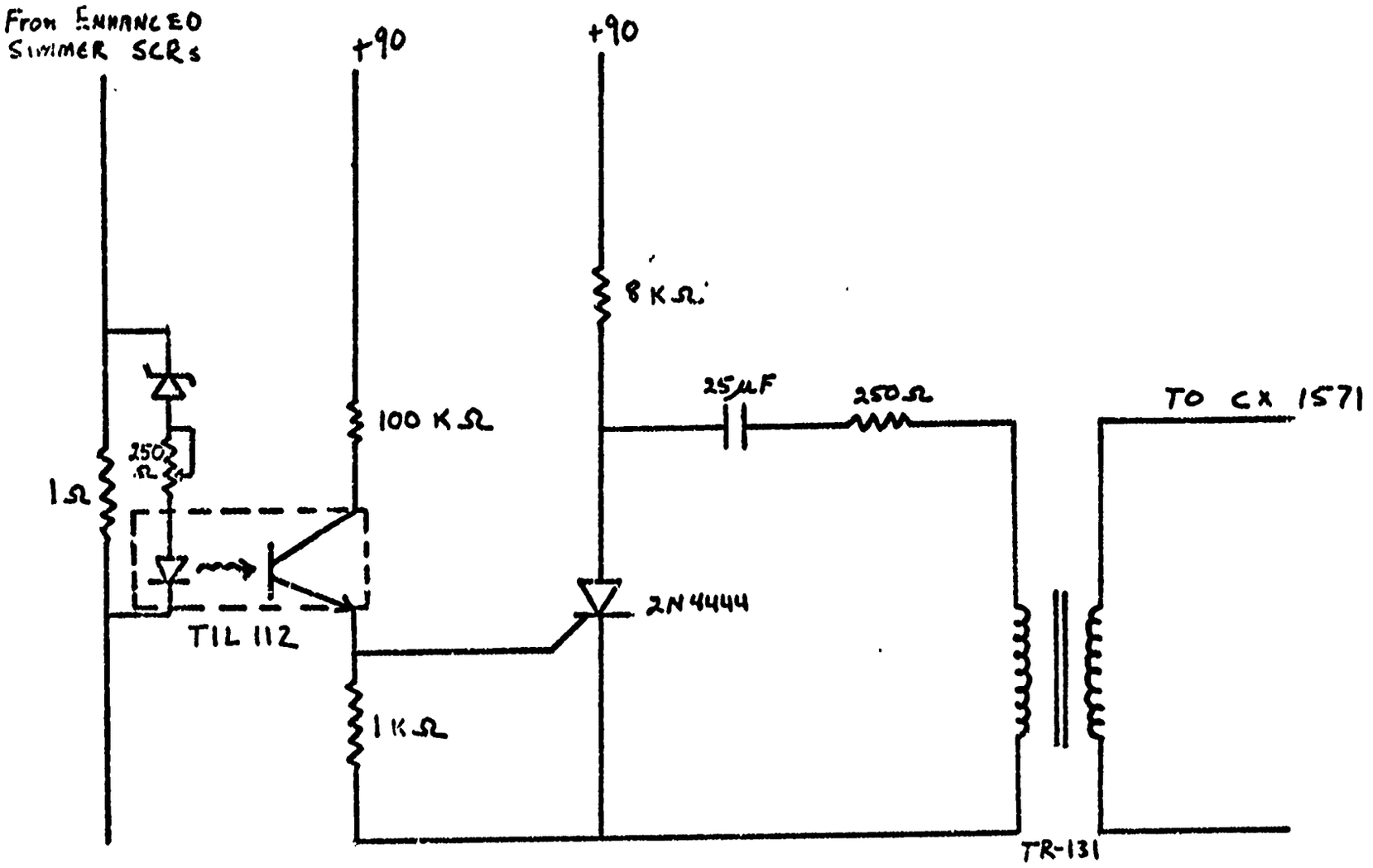
From ENHANCED SWIMMER SCRs
+90
+90
8 KΩ
25 μF
250Ω
TO CX 1571
100 KΩ
250 Ω
1Ω
2N4444
TIL 112
1 KΩ
TR-131

Fig. 5